EXHIBIT 3

**IN THE UNITED STATES COURT OF FEDERAL CLAIMS**

| | | |
|---|---|---|
| **TAYLOR ENERGY COMPANY LLC,** | ) | |
| **Plaintiff,** | ) | No. 16-12C |
| | ) | Judge Nancy B. Firestone |
| **v.** | ) | |
| **THE UNITED STATES,** | ) | |
| **Defendant.** | ) | |

**Expert Report Of Oscar Pineda-Garcia, PhD**

September 14, 2018

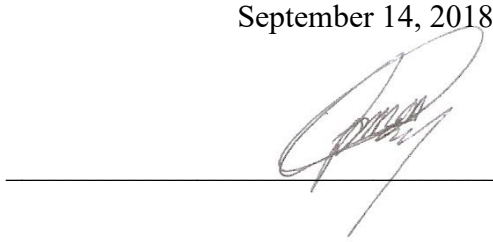

**TABLE OF CONTENTS**

1.0 Introduction

## 1.1. SCOPE OF ASSIGNMENT

I have been retained by the United States in the matter of *Taylor Energy Company, LLC v. United States of America*, (CFC No. 16-12C). More specifically, I have been asked to ascertain the amount of oil that is being discharged into the ocean from Taylor Energy Company, LLC's (Taylor's) former oil and gas lease at MC20 in the Gulf of Mexico.

## 1.2 QUALIFICATIONS AND EXPERIENCE

I am the director of Water Mapping, LLC located at 1041 Edgewater Lane, Gulf Breeze, Florida. Water Mapping, LLC is a private service provider in the area of remote sensing of oil spills. I am also an Adjunct Scientist at the Florida State University Center for Ocean-Atmospheric Prediction Studies. I am a geoscientist with more than 15 years of experience in the management of projects related to aerial and satellite remote sensing. My scope of experience has included a wide range of image processing techniques and geospatial statistical analysis for monitoring, surveying, and mapping diverse habitats or events. These have been specifically related to oil spills and the assessment of their damage to natural resources. I have actively collaborated with the U.S. National Oceanic and Atmospheric Administration (NOAA) and the Bureau of Safety and Environmental Enforcement (BSEE) in the development of image processing algorithms and technology for mapping oil spills from satellite imagery and from aerial platforms.

My curriculum vitae, which lists my publications for the past ten years is attached as Appendix A. I am being compensated at a rate of $180 per hour.

## 2.0 SUMMARY OF OPINIONS AND ORGANIZATION OF REPORT

My opinions in this matter are as follows:

Since Hurricane Ivan damaged the Taylor Energy platform there has been a persistent chronic release of oil from MC20. Since then, multiple satellites have been able to capture the magnitude of the discharge, with satellite images taken almost on a daily basis. I was asked to review the satellite imagery and to perform an analysis to estimate the rate of the volume discharge. For this task, my team and I reviewed an archive of more than one thousand satellite images collected since 2004. In this report I present the analysis of the archived imagery, in combination with the field work I have done at MC20. In this section of the report I list a summary of the conclusions of the analysis, and in the next section I present a detailed description of the observations, data, analysis, and results.

A. Based on the satellite imagery review, the site has shown floating oil 100% of the days where there has been a suitable satellite image of the area. In total, 258 satellite images spanned from 2005 to August 2018 with optimal detection conditions were analyzed; all of the images showed a slick sourced at the location of the MC20 site.
B. This suggests that the site has chronic (uninterrupted) discharge of oil.
C. The size of the oil slick ranged from 37000$m^2$ (July 6, 2005) to 385$km^2$ ( May 1$^{st}$, 2007). These measurements occurred in various conditions, from storm-gust winds to calm weather.
D. My team and I analyzed 166 images that showed the MC20 slick after the completion of the decommissioning of the six wells in 2011.
E. I have used analysis from drifters deployed at the site to estimate the resident time of the floating oil (oil lifetime) which is highly dependent on the wind strength. The average

resident time for oil throughout the events captured on the satellite imagery on six drifter deployments is 12 hours, with the resident times ranging from 6 to 17 hours.

F. Using the industry standards (Bonn Agreement), the estimated minimum daily volume discharge is of 249 Barrels with an estimated maximum of 697 Barrels per day.

G. This calculation does not account for evaporation or entrapment of the oil below the ocean surface. This means that it is likely that the actual rate of discharge from the spill site is higher than these calculations.

H. My analysis of the data shows that there is a variant flux of oil that is unrelated to external variables (oceanographic or meteorological factors).

I. Analysis on the variability of the flux for the 14 years of satellite data available shows this variability is not related to any particular seasonality. There has been an uptrend of the areas of the slick during the last two years.

J. There is significant disagreement between these calculations and the reports from United States Coast Guard's National Response Center webpage (see appendix B).

K. There have been several instances in which NRC reports estimates of floating oil during the same days that I have performed field measurements and there is abundant evidence that supports the fact that these reports from NRC are incorrect.

L. In addition to the sections included in the body of my report, I have also prepared a separate set of appendices. Appendix A is my Curriculum Vitae, Appendix B includes documentation related to industry standards (Bonn Agreement, ASTM, and NOAA), Appendix C – shows overview maps of the satellite images used on this study, Appendix D shows reference videos publically available, and finally Appendix E provides a hard copy of an article cited on this report.

M. My work in this case is ongoing and I reserve the right to adjust my analysis, calculations, and conclusions as more information becomes available.

## 3.0 VOLUME DISCHARGE CALCULATION FROM MC20 SITE.

There are multiple ways to estimate total volume of oil discharged from a chronic (fixed source) spill. For example, 1) Direct observations and measurements from devices directly installed on the seabed or near the site of discharge (e.g. sensors, videos; collection of the flux); 2) Satellite remote sensing by collecting satellite images of the spill that quantify the oil slick extent and back calculate a discharge rate from that; 3) Modeling of oil dispersion and transport, where hydrodynamic oil spill transport models are used to simulate the rate of the spill based on known initialization parameters. For this analysis I focused on the use of satellite remote sensing to estimate the flux and the rate of discharge from MC20.

Because of my research on remote sensing, I have used the MC20 site as a "natural" laboratory to evaluate the capacity of each satellite to detect oil. During this process I have had the opportunity to visit the site and perform synchronous observations and measurements at the time of multiple satellite snapshots. The objective has been to collect simultaneous measurements to test how different sensors work under a different set of conditions. Because of my scientific publications, I have been able to obtain funding to conduct multiple research experiments over the site in recent years. Although I have been visiting the site since 2009, between June 2014 to date, I have visited MC20 on 27 different days experiencing a broad range of environmental conditions and I have been able to observe the site using a variety of sensor configurations. On many of these occasions I have been joined by personnel from NOAA including Dr. Lisa DiPinto, Dr. Dan Han, and Mr. George Graettinger (senior scientists from Office of Response and Restoration, NOAA's Ocean Service), as well as personnel from the Environmental

Protection Agency (EPA), the United States Coast Guard, the National Aeronautics and Space Administration (NASA), and scientists from multiple academic institutions.

This section 3 is organized as follows. First, I describe some general observations that have been made over the site from field campaigns. Next, I describe how satellites are used to detect floating oil and its related processes; I then present a summary of the imagery and observations collected over the site during the last 14 years (spanning from November 2004 to the date of this report). Finally, I present the method for calculating the rate of the volume discharge based on the satellite imagery analysis, and the results of my analysis.

**3.1 GENERAL OBSERVATIONS OVER THE MC20.**

The MC20 site has been persistently showing releases of oil on all of the times that I have visited the area. At the main source, one can perceive the presence of hydrocarbon fumes which require the usage of respirators to operate on the surrounding areas on the site. The method shown on Figures 2 and 3 (where I get aerial support for sampling areas in synchronization with the satellite images) has been a common practice during multiple field campaigns. The next series of figures are aerial and sea level photography collected during several of the campaigns.

Figure 1 - The MC20 Spill site and the active gas fumes creating a donut where most of the gas bubbles reach the surface. This aerial photography was collected during a research cruise on June 18, 2014.

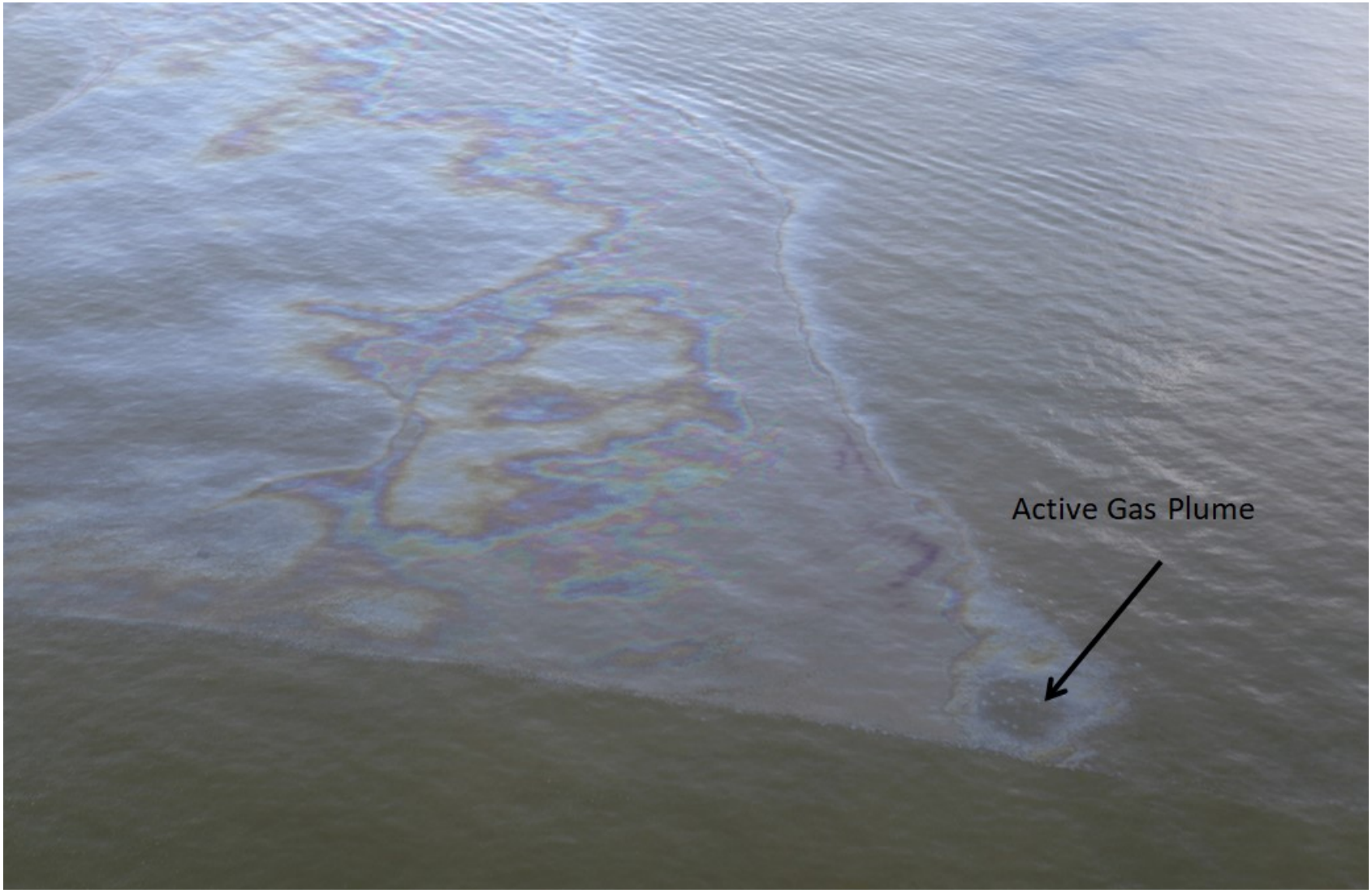

Figure 2 - This view below is from the airplane from the opposite side of the previous image. The source now appears at the upper left arrow.

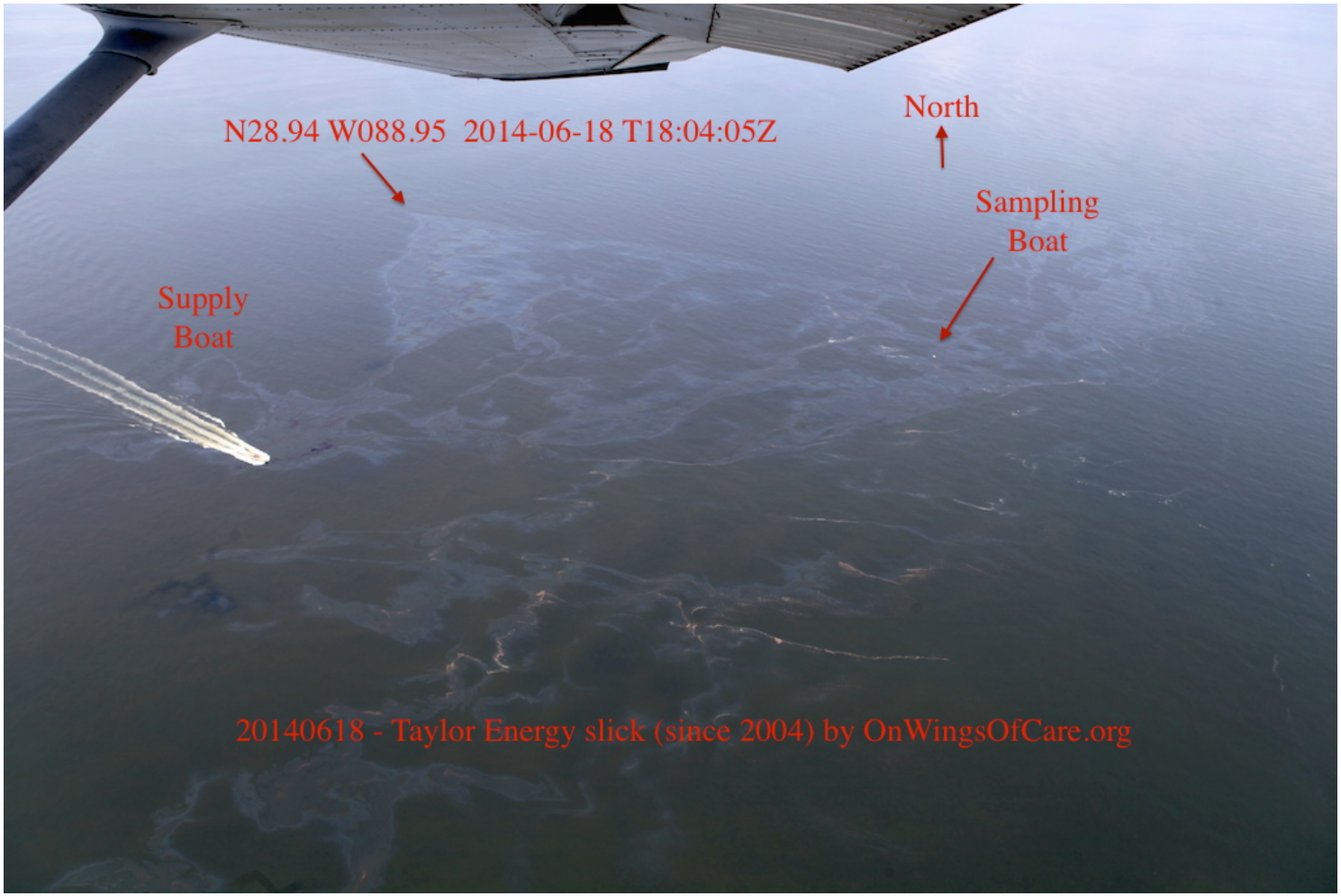


To provide a sense of scale, the white feature (Sampling Boat arrow) was a 24ft boat, and the Supply Boat was an 85ft. The distance between the source and the sampling boat was approximately 5 km.

Figure 3 - This is a closer aerial view photograph of the 24ft vessel where I was collecting samples directed by the airplane.

Figure 4 - These are samples collected during the same cruise for correlation with the satellite imagery.

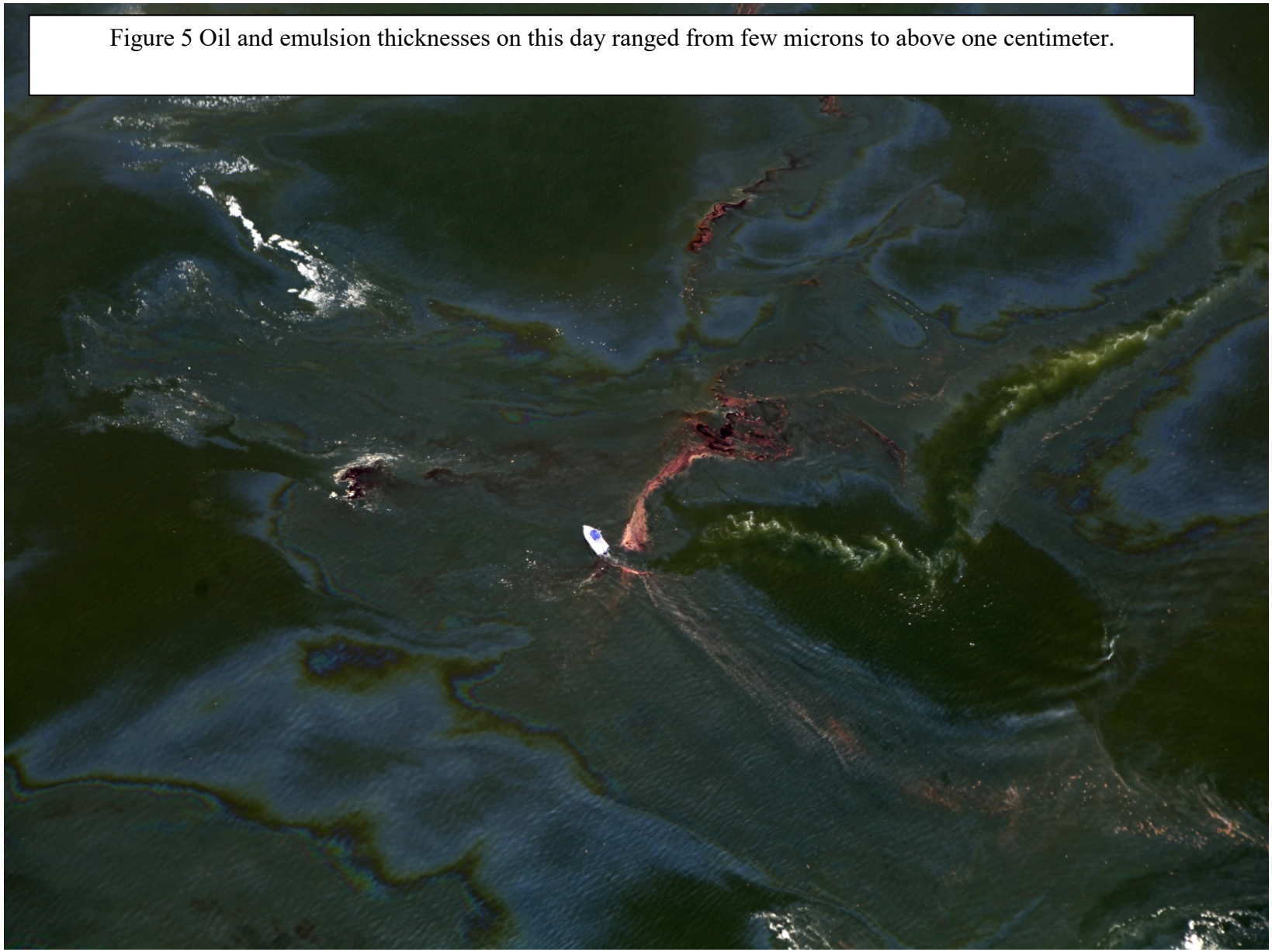

Figure 5 Oil and emulsion thicknesses on this day ranged from few microns to above one centimeter.

Fig. 6 Thick oil emulsions on the side of the sampling boat.

On recent research cruises I have been assisted by the United States Coast Guard personnel to conduct monitoring, sampling, and measuring of the MC20 oil slick. On this Figure 7 can be seen the slick in front of the USCG Brant as it is tactically positioned by the assistance of my UAS real time system. The captain of the vessel sees on real time a screen displaying a video broadcast from the drone which help us to position the boat as we perform observations of the oil slick.

On this Figure 8 we can see the USCG Brant that has been positioned right at the source of the slick.

Figure 9 shows the USCG Brant from another angle were the UAS captures the prescence of oil bubbles as they are bursting on the sea surface.

Figure 10. Samples of oil emulsions from MC20 collected on a research cruise in November 2014 were taken to the USGS laboratory in Denver to analyze its spectral characteristics and compare them to oil thicknesses from the DeepWater Horizon (DWH) spill. Top Left Sample collected by me at MC20, same sample that is being analyzed by Dr. Gregg Swayze (USGS) bottom left.

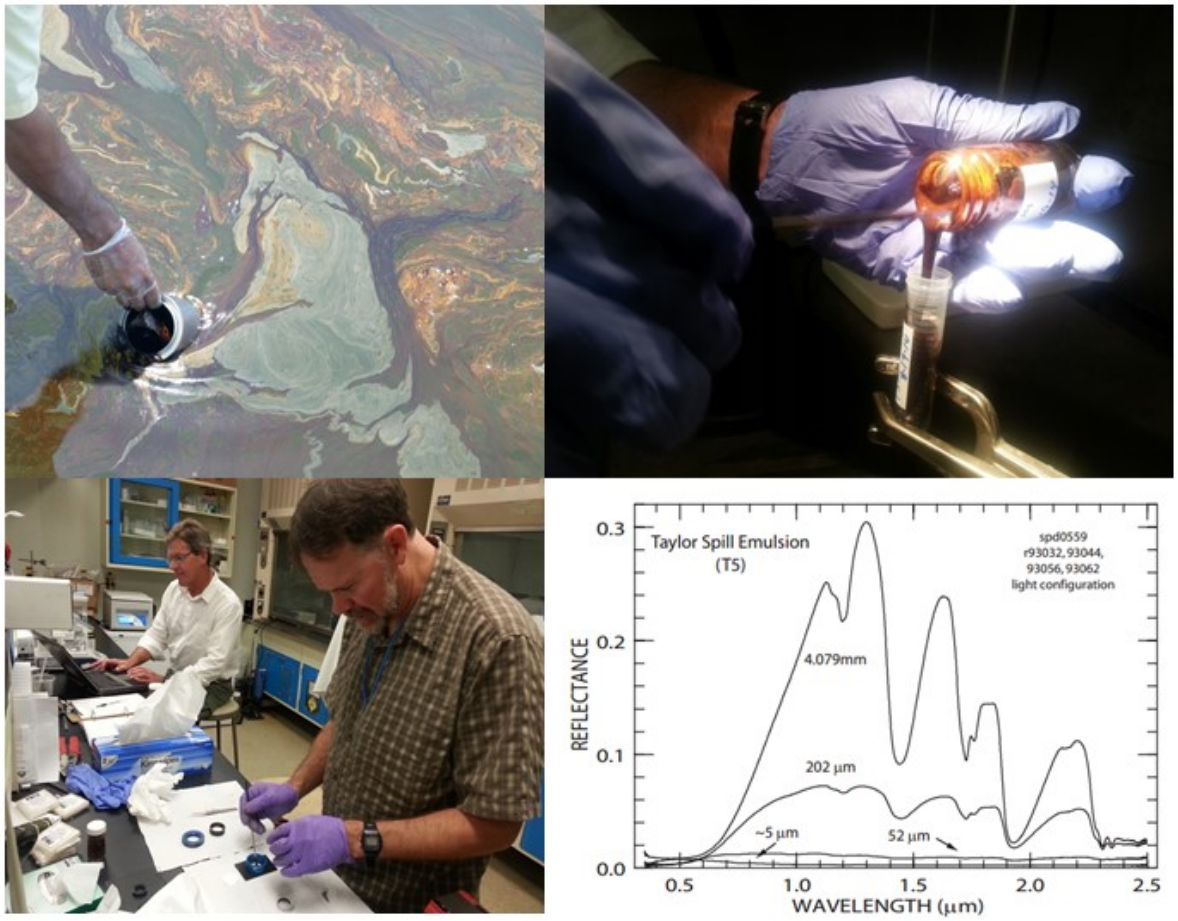

Figure 11 - This image below is from a more recent research cruise held on April 28th, 2018. The same types of features, including thick heavy emulsions, are persistently observed along the oil slick.

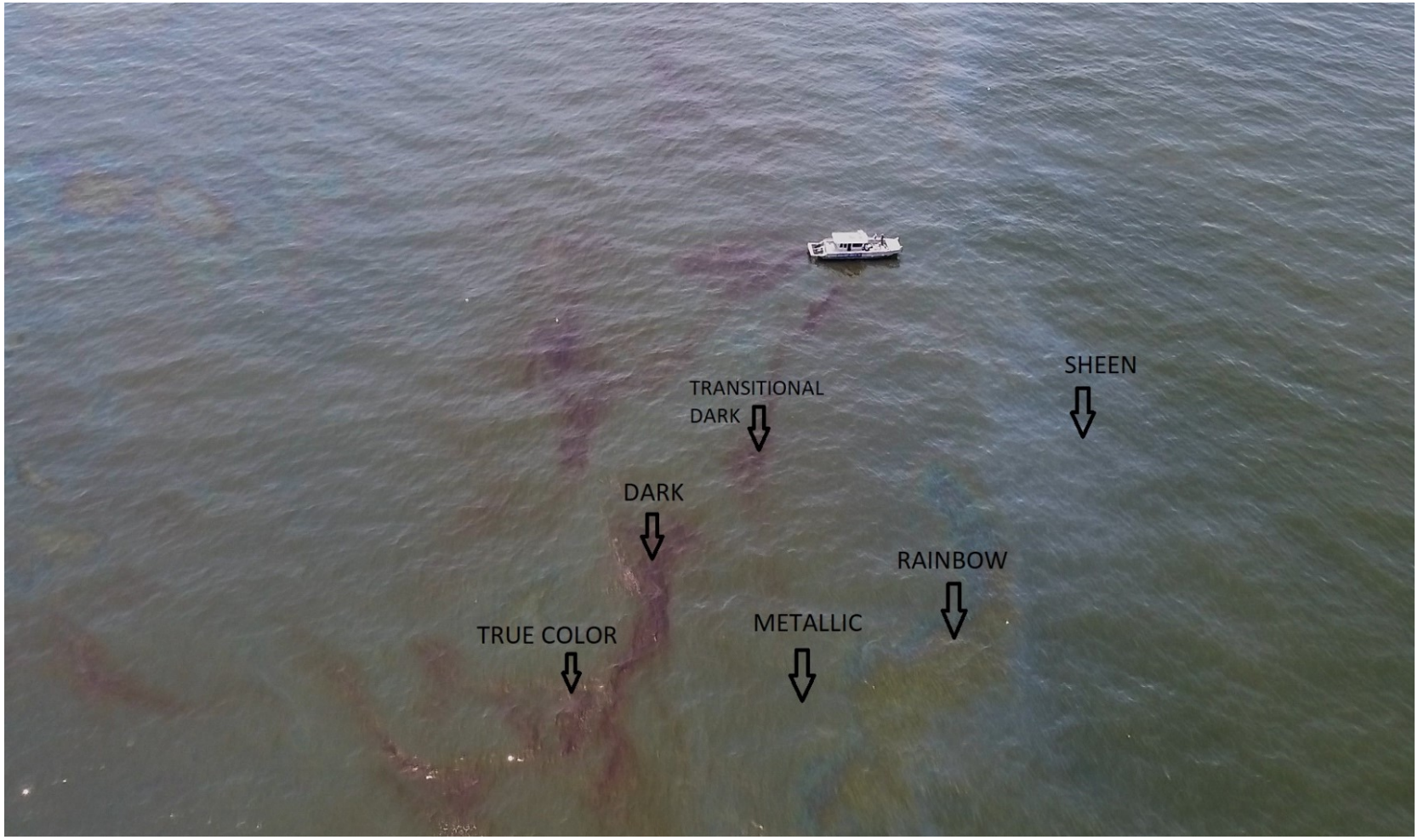

Figure 12. I have used some specialized cameras to detect the vivid aspect of the fresh oil as it reaches the surface. This UAS high resolution camera shows the oil from MC20 when it just arrived at the sea surface and creates the metallic aspect, meaning that it is thick fresh crude oil (un-emulsified). The fact that this effect is constantly seen at the source suggests that there could be a rapid discharge coming from the seafloor. This photograph was taken on another research cruise on April 20, 2017.

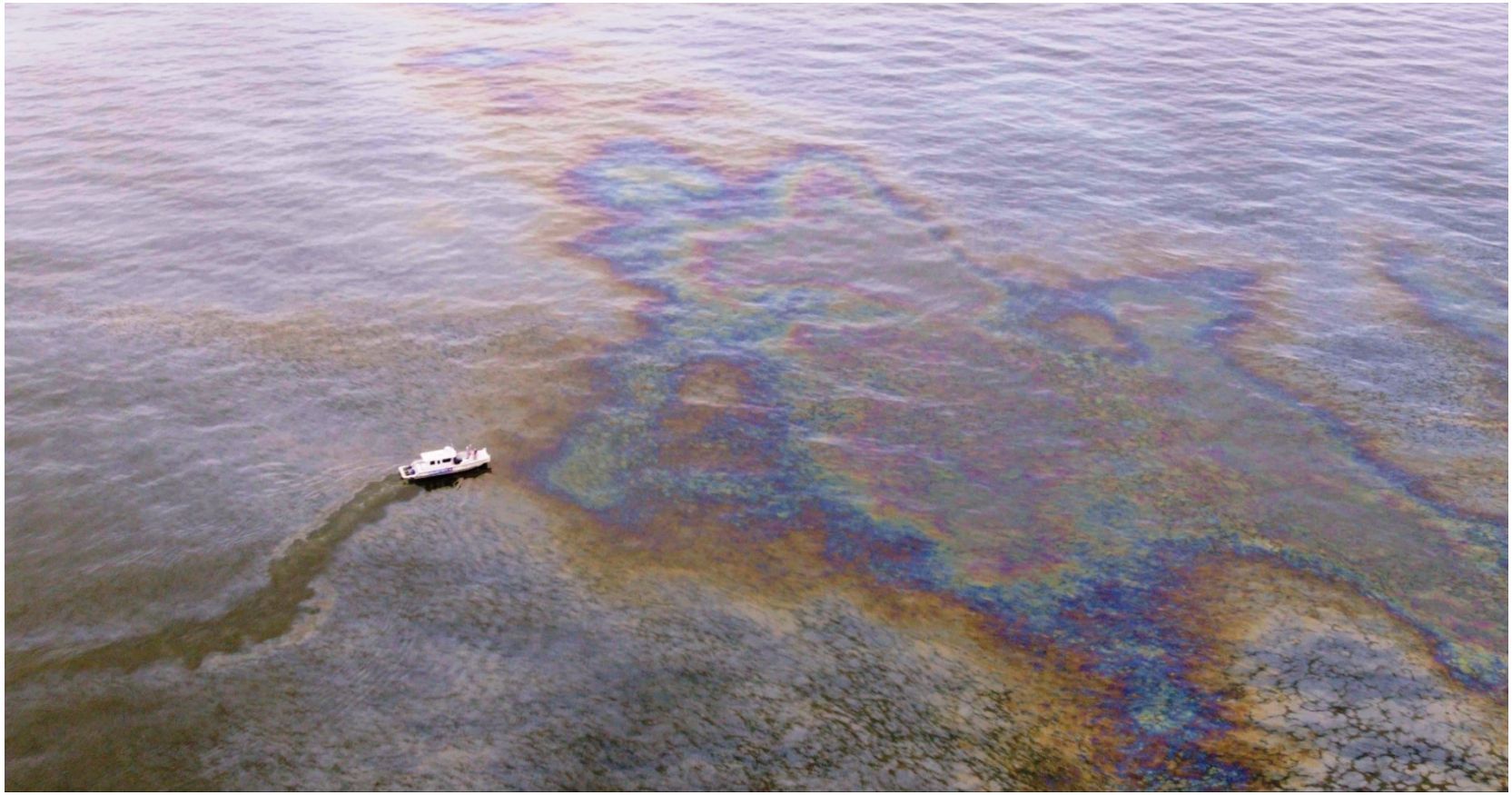

Figure 13 - This UAS aerial view is collected at the source (MC20 site) where a large amount of oil and gas bubbles reached the sea surface practically at the same time. Here, the edge of the source (diffuse boundary created by the scattered bubbles) can be observed with the clean sea water at the right of the photo. I can be seen standing on the deck getting ready to sample some of the thick fresh un-emulsified oil (metallic/true color aspect) that appears to the port side of the vessel. This image was collected on April 28th, 2018

Figure 14 - This aerial view is showing the boat from the opposite side than the previous image, when one of my colleagues (Dr. Lisa DiPinto-NOAA) is extending a pole over the port side of the vessel to collect some samples for chemical analysis. Again, this effect (the vast amount of emerging bubbles and the instant presence of thick oil at the source) suggests that there could be a rapid discharge coming from the release source at the seafloor.

Figure 15 - This sea-level photo below is taken from the boat showing the moment in which Dr. Lisa DiPinto is using the extension pole with a special net to collect a sample of the new oil that just reached the surface. (Photo was taken by Mr. Graettinger-NOAA).

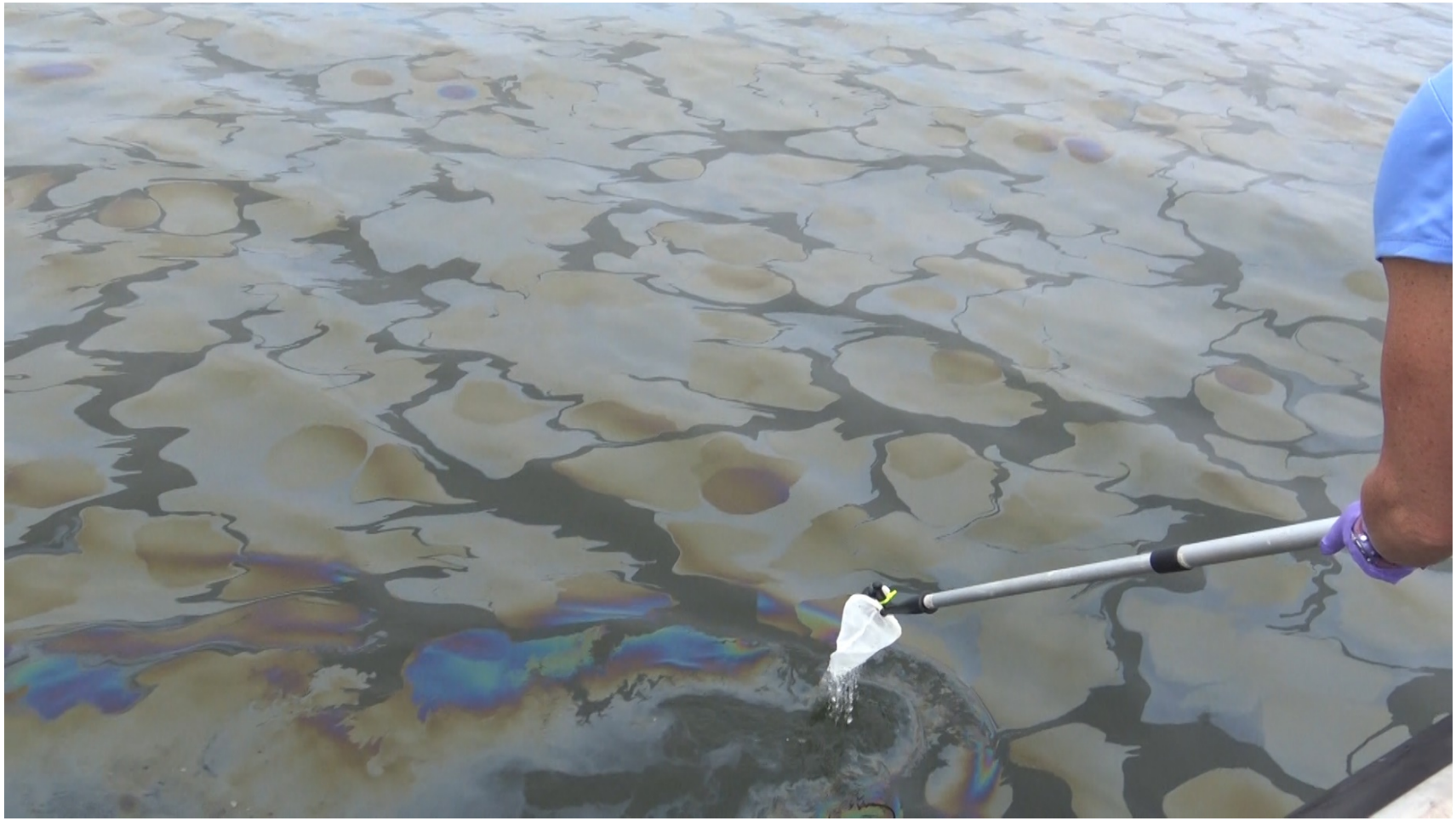

Figure 16 - This satellite image collected by satellite Sentinel-2 was collected while I was present at the site and it shows the locations of the nets collected (as shown on the previous 3 photographs). A video of the operation during this cruise can be seen:

https://youtu.be/A_f_tWtIfps

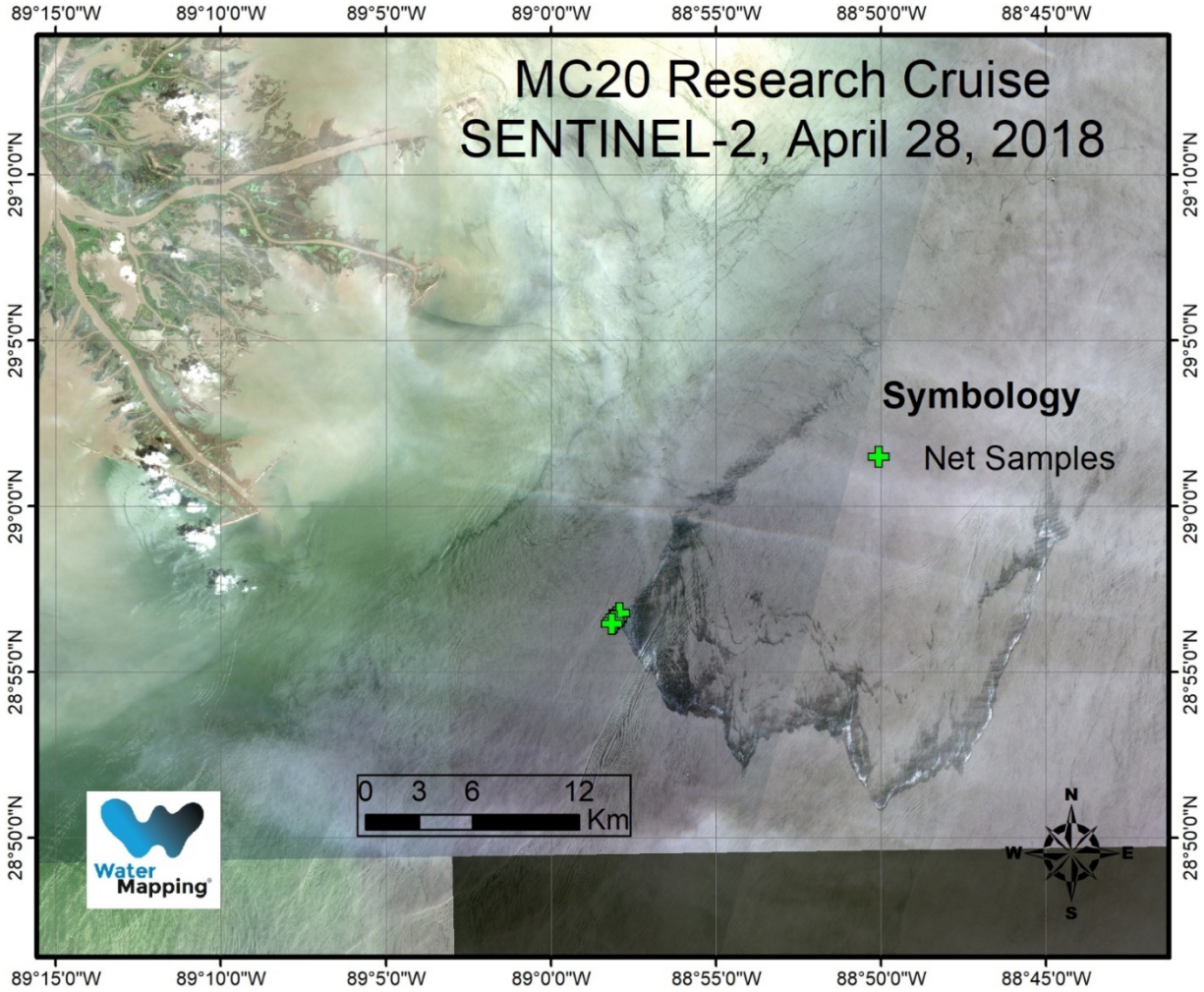

Figure 17 - This map below shows the location of the nets and a closer look at the area captured by the satellite image. Here, the thick patches of oil can be seen as the brighter color areas within the slick.

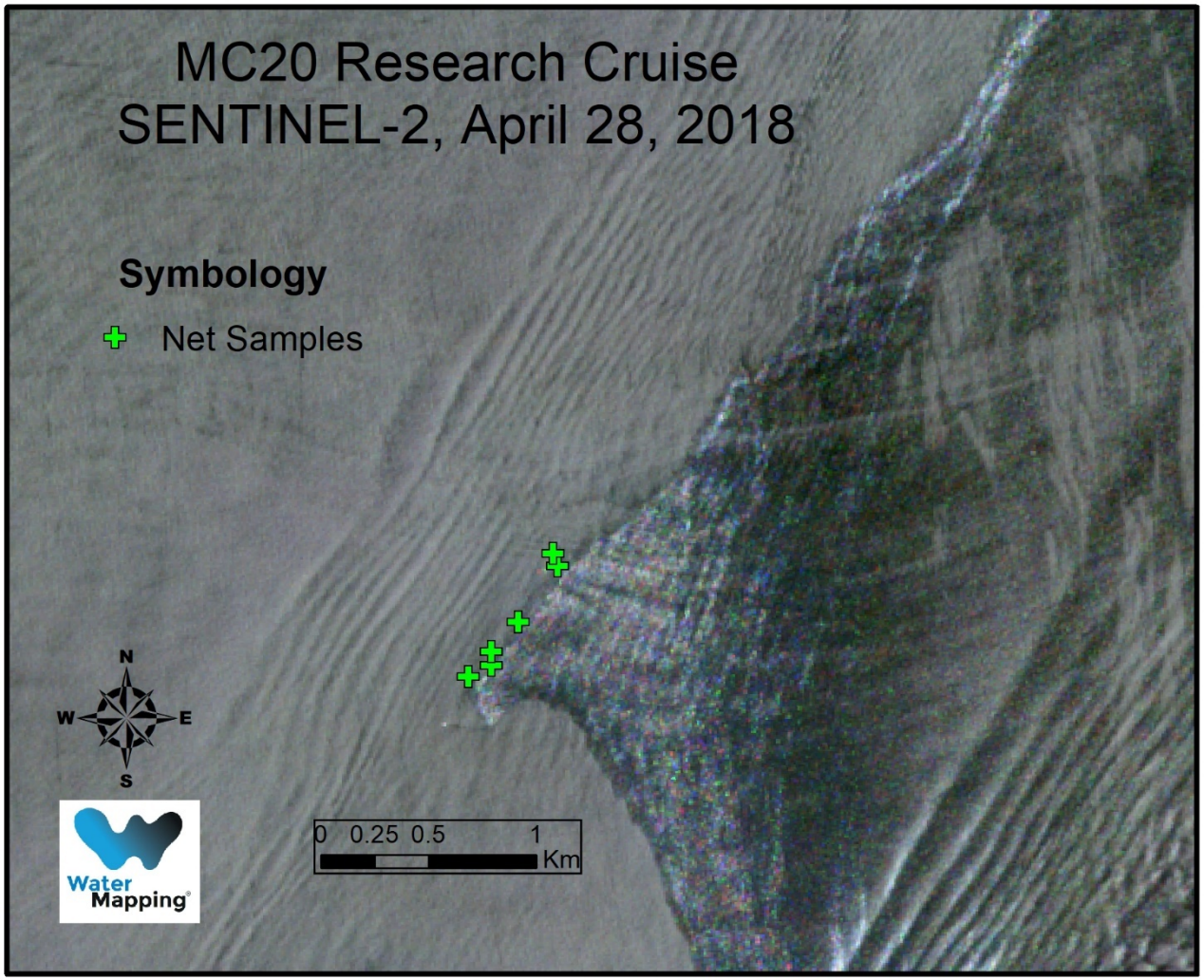

**3.2 HOW SATELLITE IMAGERY IS USED TO DETECT FLOATING OIL AT MC20.**

Remote sensing analysis techniques for oil spill detection and characterization include optical, microwave, thermal, lidar, and radar sensors mounted on aircraft and satellite platforms; from these, I focused on the application of optical and microwave satellite sensors at MC20.

The current, most advanced satellites are capable of aiming at sub-meter resolution or in multiple bands. TerraSAR-X is an X-Band Synthetic Aperture Radar (SAR) satellite, which serves as a good example of a microwave satellite that can retrieve at super high-resolution of less than 1 m per pixel. TerraSAR-X is capable of collecting an image covering hundreds of square kilometers while still being capable of retrieving features the size of a passenger motor-vehicle. RADARSAT-2 is also capable of obtaining four polarized bands on a single satellite snapshot; this means it collects four different types of SAR layers from the same image. The characteristics of these types of images allow not only the detection of absence/presence of oil, but also detection of level of emulsification of the floating layer of oil. In parallel, for the passive/optical sensors, satellites such as the WorldView 2-3-4 (which are multispectral and have at least 1 m resolution) are the best for full characterization of oil spills.

Figure 18 shows multiple satellite images collected over MC20 during a recent field study campaign. RADARSAT2 (Figure 18-A) and Advanced Spaceborne Thermal Emission and Reflection Radiometer (ASTER; Figure 18-B) images taken only few hours apart, and a WorldView2 (Figure 18-C) image collected only a few minutes after the ASTER snapshot. These images were taken over the MC20 site while I was present collecting oil slick measurements.

Figure 58 - Satellite images collected by RADARSAT-2, ASTER, and Worldview-2

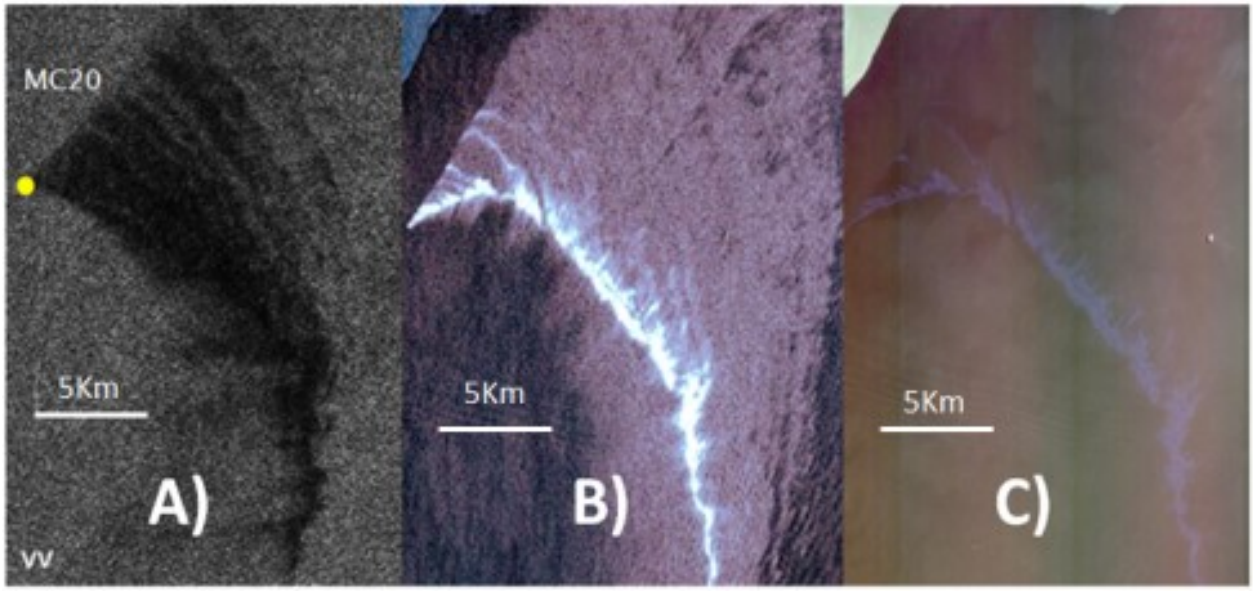


As shown in Figure 18-A, oil slicks are identified as the low backscatter from the ocean surface detected on the SAR satellite image. This low backscatter is shown as the dark area. In Figures **Error! Reference source not found.**B and **Error! Reference source not found.**C, oil slicks can be clearly visualized under limited sun glint conditions. The high frequency of these acquisitions (the three images were obtained within a four-hour timeframe) allowed the observation of a high correlation for the shape of the oil slick captured by the three satellites. Nevertheless, the viewing configurations and satellite capacities show a very different signature for the detected oil. This example showcases why it is important to understand the strengths and limitations of each of the available satellites for the detection of the oil spills. For instance, the ASTER and WorldView images are highly dependent on illumination conditions (free of cloud obstructions), sensor spatial resolution, sensor radiometric resolution, and the geometry between the viewing angles given by the relative position of the satellite with respect to the sun. This optical contrast method can be used for all collected imagery, including imagery collected from

other satellites such as the Landsat 7/8 or Sentinel 2A. Figure 18 provides a comparison of the contrast difference of the oil under different sensor capacities. Wind conditions between the satellite snapshots shown in Figure 18 were 4 m/s, on average. That is why the shape of the oil slick does not change significantly over the time between satellite images (a period of four hours). This leads to the conclusion that oil appears differently in each of the images due to the particular capabilities and specifications of each sensor. The bands and sensors used in Figure 18 were microwave from RADARSAT, and visual/multispectral from both the ASTER and WorldView 2/3.

With synoptic (occurring at the same time from multiple platforms) and frequent observations, remote sensing serves a vital role in oil spill monitoring and it can be used to assess the magnitude of a spill, especially with recent technological advancements (satellites capable of imaging features with pixel resolution of 1 m or less with multiple bandwidths). SAR has proven to be the most applicable spaceborne sensor for detecting oil spills. It enables all-weather/all-day detection with medium-to high-resolution data. Due to oil's viscoelastic properties and capacity to keep tension on the surface, it's dampening effect reduces the roughness on the water and consequently the 'Bragg scattering' in oil-covered regions, creating a distinct brightness contrast with surrounding water. The Bragg-Scattering explains the effects of the reflection of electromagnetic waves on periodic structures whose distances are in the range of a wavelength. For example, Figure 19 below shows the iteraction between the wavelength coming from a C-Band satellite over the surface of the ocean with and without oil. Capillary waves range approximately from .7cm to 10cm, and a microwave satellites signal is within that range.

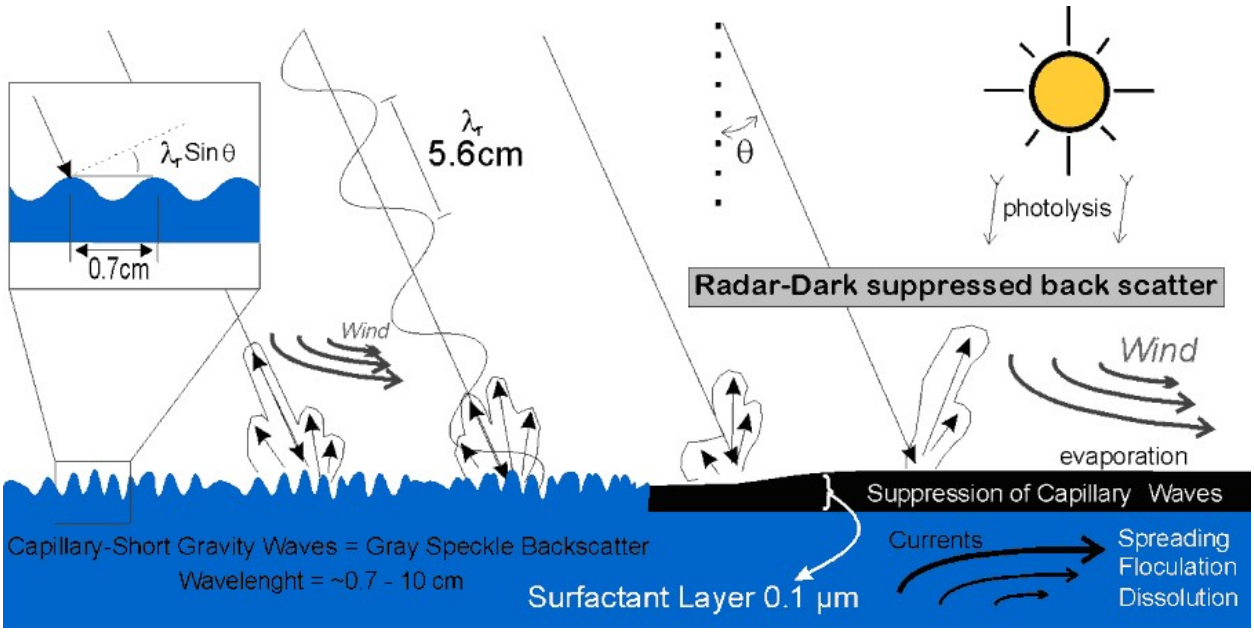


Figure 19. Oil Slicks in the water and related processes this figure source [*O Garcia-Pineda et al.*, 2009]. These concepts have been used for more than 3 decades on satellite remote sensing for detection of oil [*Alpers and Hühnerfuss*, 1988; *Gade et al.*, 1998; *Schuler et al.*, 1993; *Valenzuela*, 1978].

Passive optical remote sensing is another technique frequently used to complement SAR observations. In optical imagery, the same oil-dampening effect enables a display of positive/negative contrast between oiled surfaces and water under the proper sun glint conditions. This sun glint effect in optical remote sensing has been used to detect oil slicks on the ocean surface as shown in Figure 12. [*Hu et al.*, 2009; *Sun and Hu*, 2015; *Svejkovsky et al.*, 2016].

**3.3 DIRECT OBSERVATIONS AND MEASUREMENTS OF THE OIL SLICK.**

Figure 20 below shows an example of the planning of the missions where I study satellite imagery with direct field observations. First, using aerial support, I observe the extent of the oil slick and then I plan to collect samples of oil at different locations so I can later correlate those samples with the signature detected on the satellite imagery. Figure 20 (top) shows the aerial view of the slick and the location of samples and measurements (A, B, C, D); this snapshot was taken at the time I was transiting on a vessel from point B to C. It also shows (bottom) the snapshot collected by the satellite ASTER on May 8, 2016 at the same time as the aerial view. By doing this, we can relate the aspect of the oil on the field with the detections on the satellite images.

Figure 20 - Aerial view (top) from the slick at MC20 (photo credit: Bonny Shumaker) and satellite view (bottom) taken at the same time. The sampling site A is the origin of the MC20 spill.

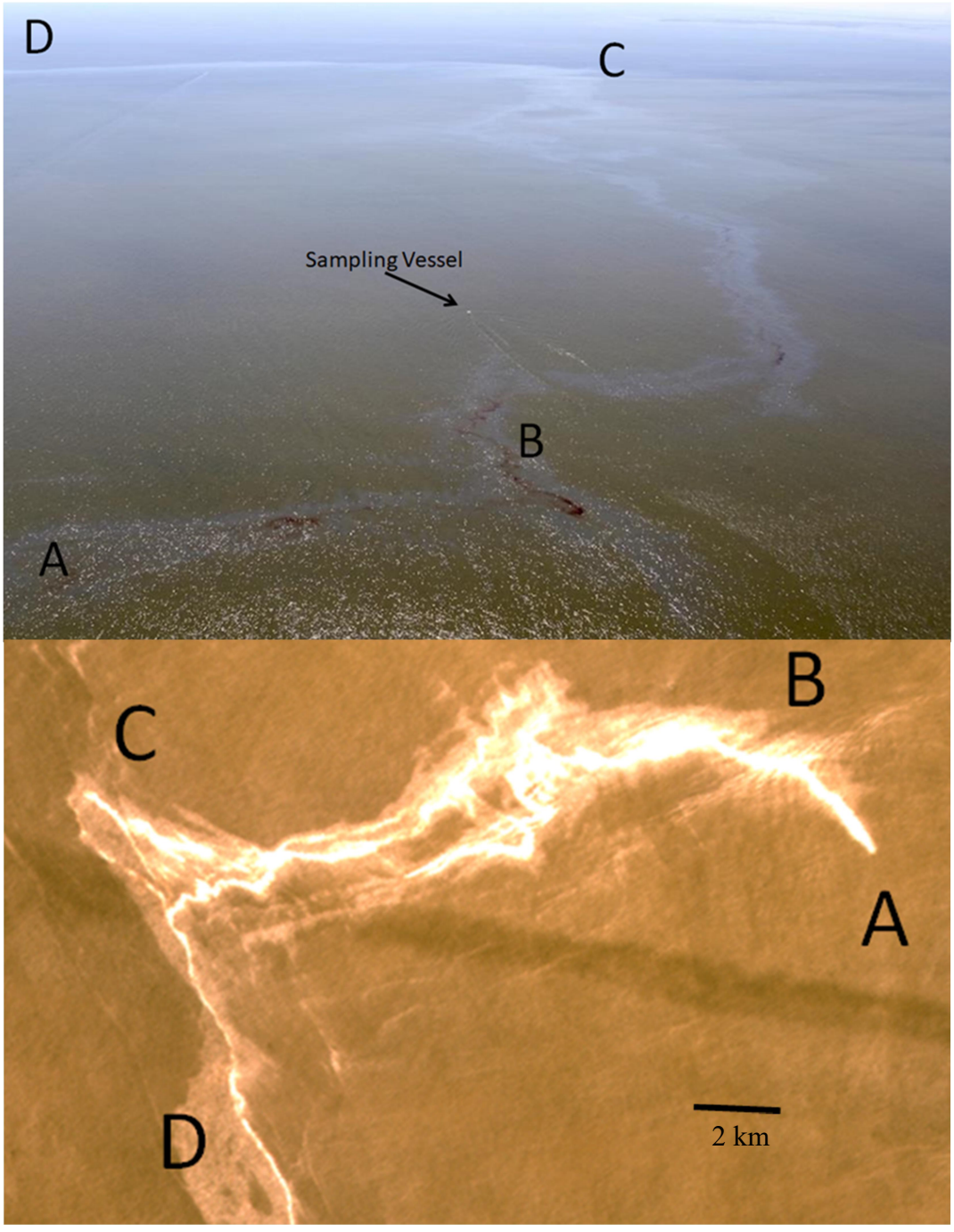

In situ observations of the oil also include thickness measurements; these are first done by visual assessment and then by collection of samples to conduct physical measurements. Figure  shows examples of the surface oil and emulsions collected at points A,B,C,D shown on the previous figures.

Figure 21 - In-situ observations of the floating oil in synchronization with the satellite images.

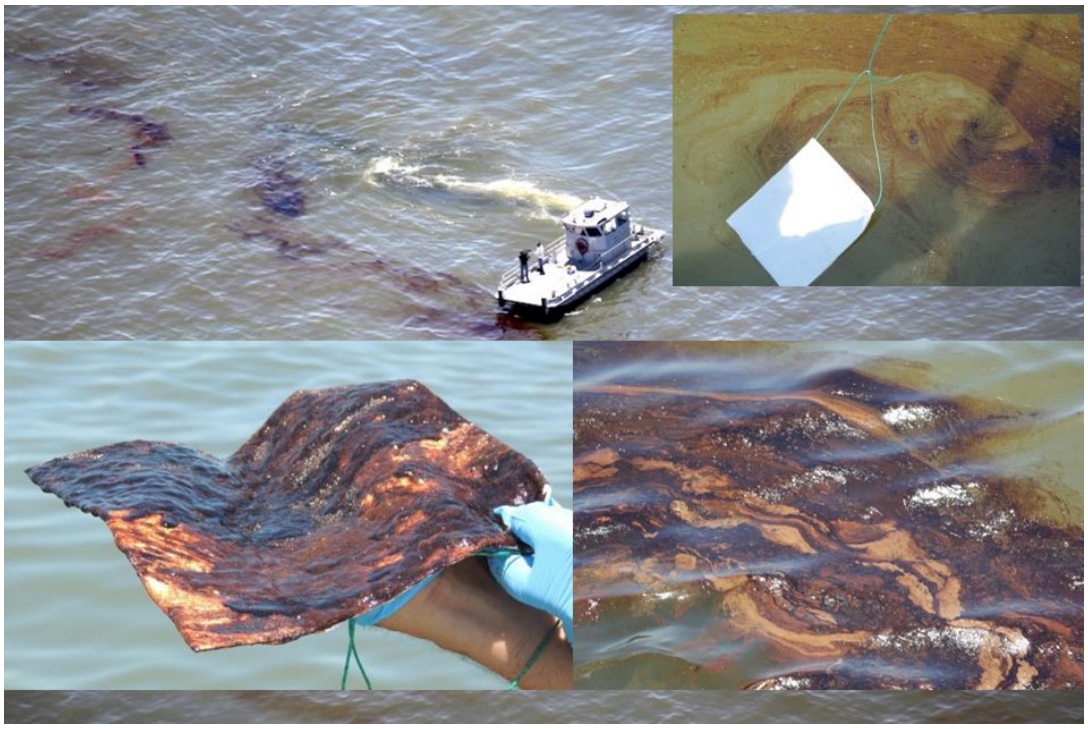

### 3.4 SATELLITE IMAGERY USED FOR THIS STUDY

As shown in Table 1, the currently available SAR microwave satellites that can be used for detection of oil the MC20 spill are high-resolution and cover multiple bands on the electromagnetic spectrum. SAR is an active remote sensing technique based on radar techniques. SAR satellite imagery have been used widely to detect the presence and absence of oil slicks under a specific window of ambient and imaging conditions, either by manually delineating radar dark areas or by using semi-automated data analysis algorithms [*Caruso et al.*, 2013; *Leifer et al.*, 2012; *MacDonald et al.*, 2015; *MDA*, 2015]. Optical remote sensing provides useful, low-cost information on oil location and surface area coverage, and it is also widely used for mapping oil spills [*Hu et al.*, 2009; *Leifer et al.*, 2012; *Sun et al.*, 2016; *Svejkovsky et al.*, 2016; *Svejkovsky et al.*, 2012].

Table 1 - Satellites available for the detection of the MC20 oil spill.

| | Satellite | Sensor Type | Spatial Resolution | Wavelength |
|---|---|---|---|---|
| Visual Multispectral | Woldview-2/3/4 | Optical | <1m | Multispectral |
| | Worldview-1 | Optical | ~1m | Multispectral |
| | Sentinel-2A/B | Optical | 10m | Multispectral |
| | Aster | Optical | 15m | Multispectral |
| | Landsat 7 | Optical | 30m | Multispectral |
| | Landsat 8 | Optical | 30m | Multispectral |
| | MODIS Terra/Aqua | Optical | 250m | Multispectral |
| SAR Microwave | Radarsat-2 | SAR | 1-50m | C-Band |
| | TerraSAR-X | SAR | 1-50m | X-Band |
| | Sentinel-1A/B | SAR | 5-40m | C-Band |
| | COSMOSKY-MED | SAR | 10-50m | X-Band |
| | ALOS-2 | SAR | 5-40m | L-Band |

Passive optical remote sensing is a frequently used technique that can complement SAR observations, but it depends heavily on the sun's illumination. In other words, if we think about the ocean as a reflector (like a mirror), a lot of the illumination that the sun provides is reflected by the sea surface and sent back to the space. If an optical satellite is in the right position, it should capture this specular reflection of the sun, also called the sun glint effect. In optical imagery, the same oil dampening effect enables a display of positive/negative contrast between oiled surfaces and water under proper sun glint conditions. An image analyst with the proper background and training and the ability to look at the satellite images in their highest resolution can enhance the contrast of the sea surface and look for any variance on the pixel values. If a feature appears in an unusual area, this region is subjected to further investigation to determine the source of the anomaly. Table 2 (next) is a list of the images used in this analysis. Here I show the date of the satellite acquisition and the measured area of the slick extent. Appendix C contains an overview map of each of the images analyzed. Because the DeepWater-Horizon oil spill occurred in 2010 and lasted for several months, I have excluded this entire year from the analysis.

Table 2 – List of images used in this analysis

| Date | Landsat l5 | Landsat l7 | Landsat l8 | Sentinel 1 | Sentinel 2 | ASTER | RADARSAT | TERRA SAR | world view | envisat | ers E2 | total | Area Km2 |
|---|---|---|---|---|---|---|---|---|---|---|---|---|---|
| 3/24/2005 | 1 | | | | | | | | | | | 1 | 36.02 |
| 4/9/2005 | 1 | | | | | | | | | | | 1 | 1.56 |
| 4/17/2005 | | 1 | | | | | | | | | | 1 | 31.57 |
| 5/11/2005 | 1 | | | | | | | | | | | 1 | 3.10 |
| 5/19/2005 | | 1 | | | | | | | | | | 1 | 34.77 |
| 5/27/2005 | 1 | | | | | | | | | | | 1 | 62.57 |
| 6/4/2005 | | 1 | | | | | | | | | | 1 | 9.59 |
| 6/20/2005 | | 1 | | | | | | | | | | 1 | 24.79 |
| 7/6/2005 | | 1 | | | | | | | | | | 1 | 0.04 |
| 7/14/2005 | 1 | | | | | | | | | | | 1 | 12.63 |
| 8/15/2005 | 1 | | | | | | | | | | | 1 | 133.31 |
| 10/11/2005 | | | | | | | | | | 1 | | 1 | 16.47 |
| 2/15/2006 | | | 1 | | | | | | | | | 1 | 0.40 |
| 3/16/2006 | | | | | | | | | | 1 | | 1 | 20.28 |
| 3/19/2006 | | 1 | | | | | | | | | | 1 | 14.24 |
| 4/20/2006 | | 1 | | | | | | | | | | 1 | 8.80 |
| 4/20/2006 | | | | | | | | | | 1 | | 1 | 0.16 |
| 4/28/2006 | 1 | | | | | | | | | | | 1 | 8.22 |
| 5/6/2006 | | 1 | | | | | | | | | | 1 | 49.05 |
| 5/14/2006 | 1 | | | | | | | | | | | 1 | 23.97 |
| 5/30/2006 | 1 | | | | | | | | | | | 1 | 50.68 |
| 6/15/2006 | 1 | | | | | | | | | | | 1 | 118.07 |
| 6/23/2006 | | 1 | | | | | | | | | | 1 | 5.03 |
| 8/2/2006 | 1 | | | | | | | | | | | 1 | 82.59 |
| 9/3/2006 | 1 | | | | | | | | | | | 1 | 278.33 |
| 9/11/2006 | | 1 | | | | | | | | | | 1 | 11.63 |
| 10/5/2006 | 1 | | | | | | | | | | | 1 | 7.48 |
| 11/14/2006 | | 1 | | | | | | | | | | 1 | 23.56 |
| 11/22/2006 | 1 | | | | | | | | | | | 1 | 0.32 |
| 1/25/2007 | 1 | | | | | | | | | | | 1 | 1.42 |
| 3/6/2007 | | 1 | | | | | | | | | | 1 | 10.00 |
| 4/23/2007 | | 1 | | | | | | | | | | 1 | 10.09 |
| 5/1/2007 | 1 | | | | | | | | | | | 1 | 385.70 |
| 5/9/2007 | | 1 | | | | | | | | | | 1 | 26.88 |
| 5/25/2007 | | 1 | | | | | | | | | | 1 | 1.13 |

| Date | Landsat l5 | Landsat l7 | Landsat l8 | Sentinel 1 | Sentinel 2 | ASTER | RADARSAT | TERRA SAR | world view | envisat | ers E2 | total | Area Km2 |
|---|---|---|---|---|---|---|---|---|---|---|---|---|---|
| 6/2/2007 | 1 | | | | | | | | | | | 1 | 1.19 |
| 6/10/2007 | | 1 | | | | | | | | | | 1 | 2.69 |
| 7/4/2007 | 1 | | | | | | | | | | | 1 | 6.09 |
| 8/5/2007 | 1 | | | | | | | | | | | 1 | 59.70 |
| 8/13/2007 | | 1 | | | | | | | | | | 1 | 70.09 |
| 8/21/2007 | 1 | | | | | | | | | | | 1 | 4.49 |
| 8/29/2007 | | 1 | | | | | | | | | | 1 | 66.58 |
| 9/6/2007 | 1 | | | | | | | | | | | 1 | 35.44 |
| 9/22/2007 | 1 | | | | | | | | | | | 1 | 1.68 |
| 10/13/2007 | | | | | | | | | | 1 | | 1 | 27.60 |
| 10/16/2007 | | | | | | | | | | 1 | | 1 | 0.93 |
| 11/1/2007 | | 1 | | | | | | | | | | 1 | 2.80 |
| 11/20/2007 | | | | | | | | | | 1 | | 1 | 1.49 |
| 12/6/2007 | | | | | | | | | | 1 | | 1 | 40.63 |
| 12/22/2007 | | | | | | | | | | 1 | | 1 | 0.78 |
| 1/29/2008 | | | | | | | | | | 1 | | 1 | 23.43 |
| 2/5/2008 | | 1 | | | | | | | | | | 1 | 3.73 |
| 2/14/2008 | | | | | | | | | | 1 | | 1 | 1.43 |
| 3/17/2008 | 1 | | | | | | | | | | | 1 | 0.34 |
| 4/2/2008 | 1 | | | | | | | | | | | 1 | 0.45 |
| 4/8/2008 | | | | | | | | | | 1 | | 1 | 3.06 |
| 4/10/2008 | | 1 | | | | | | | | | | 1 | 1.26 |
| 4/18/2008 | 1 | | | | | | | | | | | 1 | 2.15 |
| 5/12/2008 | | 1 | | | | | | | | | | 1 | 2.62 |
| 5/20/2008 | 1 | | | | | | | | | | | 1 | 21.71 |
| 5/28/2008 | | 1 | | | | | | | | | | 1 | 5.93 |
| 6/5/2008 | 1 | | | | | | | | | | | 1 | 2.44 |
| 6/13/2008 | | 1 | | | | | | | | | | 1 | 195.52 |
| 6/21/2008 | 1 | | | | | | | | | | | 1 | 20.00 |
| 6/29/2008 | | 1 | | | | | | | | | | 1 | 2.46 |
| 8/8/2008 | 1 | | | | | | | | | | | 1 | 62.92 |
| 9/9/2008 | 1 | | | | | | | | | | | 1 | 89.79 |
| 10/3/2008 | | 1 | | | | | | | | | | 1 | 28.02 |
| 10/19/2008 | | 1 | | | | | | | | | | 1 | 1.57 |
| 11/20/2008 | | 1 | | | | | | | | | | 1 | 3.79 |
| 1/22/2009 | | 1 | | | | | | | | | | 1 | 36.37 |

| Date | Landsat l5 | Landsat l7 | Landsat l8 | Sentinel 1 | Sentinel 2 | ASTER | RADARSAT | TERRA SAR | world view | envisat | ers E2 | total | Area Km2 |
|---|---|---|---|---|---|---|---|---|---|---|---|---|---|
| 2/7/2009 | | 1 | | | | | | | | | | 1 | 8.78 |
| 3/11/2009 | | 1 | | | | | | | | | | 1 | 5.57 |
| 3/19/2009 | 1 | | | | | | | | | | | 1 | 0.77 |
| 4/4/2009 | 1 | | | | | | | | | | | 1 | 8.69 |
| 4/28/2009 | | 1 | | | | | | | | | | 1 | 18.80 |
| 5/6/2009 | 1 | | | | | | | | | | | 1 | 0.89 |
| 5/14/2009 | | 1 | | | | | | | | | | 1 | 20.27 |
| 5/30/2009 | | 1 | | | | | | | | | | 1 | 97.95 |
| 6/7/2009 | 1 | | | | | | | | | | | 1 | 42.32 |
| 6/15/2009 | | 1 | | | | | | | | | | 1 | 75.68 |
| 6/23/2009 | 1 | | | | | | | | | | | 1 | 21.67 |
| 7/1/2009 | | 1 | | | | | | | | | | 1 | 103.70 |
| 7/9/2009 | 1 | | | | | | | | | | | 1 | 0.53 |
| 8/2/2009 | | 1 | | | | | | | | | | 1 | 24.66 |
| 8/26/2009 | 1 | | | | | | | | | | | 1 | 7.35 |
| 9/3/2009 | | 1 | | | | | | | | | | 1 | 3.32 |
| 9/19/2009 | | 1 | | | | | | | | | | 1 | 5.68 |
| 10/13/2009 | 1 | | | | | | | | | | | 1 | 8.31 |
| 11/6/2009 | | 1 | | | | | | | | | | 1 | 6.32 |
| 1/12/2011 | | 1 | | | | | | | | | | 1 | 0.80 |
| 2/21/2011 | 1 | | | | | | | | | | | 1 | 0.40 |
| 3/25/2011 | 1 | | | | | | | | | | | 1 | 92.89 |
| 4/2/2011 | | 1 | | | | | | | | | | 1 | 59.14 |
| 4/10/2011 | 1 | | | | | | | | | | | 1 | 20.82 |
| 4/18/2011 | | 1 | | | | | | | | | | 1 | 2.29 |
| 5/4/2011 | | 1 | | | | | | | | | | 1 | 0.11 |
| 5/12/2011 | 1 | | | | | | | | | | | 1 | 35.07 |
| 5/20/2011 | | 1 | | | | | | | | | | 1 | 1.95 |
| 5/28/2011 | 1 | | | | | | | | | | | 1 | 19.31 |
| 6/13/2011 | 1 | | | | | | | | | | | 1 | 138.90 |
| 6/29/2011 | 1 | | | | | | | | | | | 1 | 2.43 |
| 7/31/2011 | 1 | | | | | | | | | | | 1 | 3.12 |
| 8/16/2011 | 1 | | | | | | | | | | | 1 | 19.00 |
| 8/24/2011 | | 1 | | | | | | | | | | 1 | 13.25 |
| 9/9/2011 | | 1 | | | | | | | | | | 1 | 31.29 |
| 10/3/2011 | 1 | | | | | | | | | | | 1 | 0.33 |
| 10/27/2011 | | 1 | | | | | | | | | | 1 | 1.01 |

| Date | Landsat l5 | Landsat l7 | Landsat l8 | Sentinel 1 | Sentinel 2 | ASTER | RADARSAT | TERRA SAR | world view | envisat | ers E2 | total | Area Km2 |
|---|---|---|---|---|---|---|---|---|---|---|---|---|---|
| 2 0 1 2 | | | | | | | | | | | | | |
| 4/21/2012 | | 1 | | | | | | | | | | 1 | 51.67 |
| 5/23/2012 | | 1 | | | | | | | | | | 1 | 11.70 |
| 6/8/2012 | | 1 | | | | | | | | | | 1 | 106.91 |
| 7/26/2012 | | 1 | | | | | | | | | | 1 | 2.46 |
| 8/11/2012 | | 1 | | | | | | | | | | 1 | 5.76 |
| 8/27/2012 | | 1 | | | | | | | | | | 1 | 9.01 |
| 9/12/2012 | | 1 | | | | | | | | | | 1 | 1.03 |
| 9/28/2012 | | 1 | | | | | | | | | | 1 | 35.48 |
| 10/14/2012 | | 1 | | | | | | | | | | 1 | 24.84 |
| 11/15/2012 | | 1 | | | | | | | | | | 1 | 1.65 |
| 3/6/2013 | | 1 | | | | | | | | | | 1 | 2.43 |
| 4/7/2013 | | 1 | | | | | | | | | | 1 | 19.94 |
| 4/23/2013 | | 1 | | | | | | | | | | 1 | 3.48 |
| 5/1/2013 | | | 1 | | | | | | | | | 1 | 2.90 |
| 5/9/2013 | | 1 | | | | | | | | | | 1 | 6.27 |
| 5/17/2013 | | | 1 | | | | | | | | | 1 | 9.83 |
| 5/25/2013 | | 1 | | | | | | | | | | 1 | 7.13 |
| 6/18/2013 | | | 1 | | | | | | | | | 1 | 34.76 |
| 8/5/2013 | | | 1 | | | | | | | | | 1 | 33.03 |
| 8/13/2013 | | 1 | | | | | | | | | | 1 | 10.28 |
| 8/21/2013 | | | 1 | | | | | | | | | 1 | 25.54 |
| 8/29/2013 | | 1 | | | | | | | | | | 1 | 61.38 |
| 9/14/2013 | | 1 | | | | | | | | | | 1 | 4.10 |
| 11/9/2013 | | | 1 | | | | | | | | | 1 | 1.42 |
| 12/3/2013 | | 1 | | | | | | | | | | 1 | 3.81 |
| 1/12/2014 | | | 1 | | | | | | | | | 1 | 16.91 |
| 3/1/2014 | | | 1 | | | | | | | | | 1 | 7.31 |
| 3/25/2014 | | 1 | | | | | | | | | | 1 | 0.55 |
| 4/10/2014 | | 1 | | | | | | | | | | 1 | 6.73 |
| 4/26/2014 | | 1 | | | | | | | | | | 1 | 93.35 |
| 5/4/2014 | | | 1 | | | | | | | | | 1 | 20.21 |
| 5/12/2014 | | 1 | | | | | | | | | | 1 | 6.18 |
| 5/20/2014 | | | 1 | | | | | | | | | 1 | 30.83 |
| 6/21/2014 | | | 1 | | | | | | | | | 1 | 44.60 |
| 6/29/2014 | | 1 | | | | | | | | | | 1 | 50.17 |

| Date | Landsat l5 | Landsat l7 | Landsat l8 | Sentinel 1 | Sentinel 2 | ASTER | RADARSAT | TERRA SAR | world view | envisat | ers E2 | total | Area Km2 |
|---|---|---|---|---|---|---|---|---|---|---|---|---|---|
| 7/7/2014 | | | 1 | | | | | | | | | 1 | 12.37 |
| 7/31/2014 | | 1 | | | | | | | | | | 1 | 136.34 |
| 8/8/2014 | | | 1 | | | | | | | | | 1 | 3.48 |
| 8/16/2014 | | 1 | | | | | | | | | | 1 | 13.80 |
| 8/24/2014 | | | 1 | | | | | | | | | 1 | 3.21 |
| 9/1/2014 | | 1 | | | | | | | | | | 1 | 5.76 |
| 9/9/2014 | | | 1 | | | | | | | | | 1 | 9.59 |
| 9/17/2014 | | 1 | | | | | | | | | | 1 | 1.44 |
| 10/27/2014 | | | 1 | | | | | | | | | 1 | 22.61 |
| 11/28/2014 | | | 1 | | | | | | | | | 1 | 24.25 |
| 12/6/2014 | | 1 | | | | | | | | | | 1 | 1.26 |
| 1/7/2015 | | 1 | | | | | | | | | | 1 | 5.80 |
| 2/8/2015 | | 1 | | | | | | | | | | 1 | 2.96 |
| 3/20/2015 | | | 1 | | | | | | | | | 1 | 14.98 |
| 3/28/2015 | | 1 | | | | | | | | | | 1 | 8.07 |
| 5/7/2015 | | | 1 | | | | | | | | | 1 | 15.25 |
| 5/23/2015 | | | 1 | | | | | | | | | 1 | 3.53 |
| 5/31/2015 | | 1 | | | | | | | | | | 1 | 28.95 |
| 6/8/2015 | | | 1 | | | | | | | | | 1 | 58.55 |
| 6/16/2015 | | 1 | | | | | | | | | | 1 | 1.29 |
| 6/24/2015 | | | 1 | | | | | | | | | 1 | 49.69 |
| 7/10/2015 | | | 1 | | | | | | | | | 1 | 102.33 |
| 7/26/2015 | | | 1 | | | | | | | | | 1 | 24.60 |
| 8/11/2015 | | | 1 | | | | | | | | | 1 | 5.64 |
| 8/19/2015 | | 1 | | | | | | | | | | 1 | 1.74 |
| 8/27/2015 | | | 1 | | | | | | | | | 1 | 3.96 |
| 9/20/2015 | | 1 | | | | | | | | | | 1 | 37.33 |
| 9/28/2015 | | | 1 | | | | | | | | | 1 | 0.37 |
| 10/14/2015 | | | 1 | | | | | | | | | 1 | 7.42 |
| 10/30/2015 | | | 1 | | | | | | | | | 1 | 5.96 |
| 11/23/2015 | | 1 | | | | | | | | | | 1 | 0.74 |
| 12/9/2015 | | 1 | | | | | | | | | | 1 | 10.48 |
| 12/25/2015 | | 1 | | | | | | | | | | 1 | 5.81 |
| 12/25/2015 | | | | | 1 | | | | | | | 1 | 5.81 |
| 1/5/2016 | | | | | 1 | | | | | | | 1 | 4.58 |
| 1/18/2016 | | | 1 | | | | | | | | | 1 | 6.86 |

| Date | Landsat l5 | Landsat l7 | Landsat l8 | Sentinel 1 | Sentinel 2 | ASTER | RADARSAT | TERRA SAR | world view | envisat | ers E2 | total | Area Km2 |
|---|---|---|---|---|---|---|---|---|---|---|---|---|---|
| 1/18/2016 | | | | 1 | | | | | | | | 1 | 3.46 |
| 1/27/2016 | | | | | 1 | | | | | | | 1 | 13.34 |
| 1/28/2016 | | | | 1 | | | | | | | | 1 | 3.46 |
| 2/15/2016 | | | | | 1 | | | | | | | 1 | 3.13 |
| 3/7/2016 | | | 1 | | | | | | | | | 1 | 1.26 |
| 3/15/2016 | | | | | 1 | | | | | | | 1 | 11.18 |
| 3/28/2016 | | | | 1 | | | | | | | | 1 | 0.77 |
| 4/8/2016 | | | 1 | | | | | | | | | 1 | 9.03 |
| 4/23/2016 | | | | | 1 | | | | | | | 1 | 39.09 |
| 4/24/2016 | | | 1 | | | | | | | | | 1 | 35.97 |
| 5/2/2016 | | 1 | | | | | | | | | | 1 | 6.55 |
| 5/4/2016 | | | | | 1 | | | | | | | 1 | 1.81 |
| 5/14/2016 | | | | | 1 | | | | | | | 1 | 2.19 |
| 5/23/2016 | | | | | 1 | | | | | | | 1 | 2.86 |
| 5/26/2016 | | | 1 | | | | | | | | | 1 | 8.41 |
| 6/3/2016 | | 1 | | | | | | | | | | 1 | 120.62 |
| 6/11/2016 | | | 1 | | | | | | | | | 1 | 4.49 |
| 6/23/2016 | | | | | 1 | | | | | | | 1 | 32.58 |
| 7/2/2016 | | | | | 1 | | | | | | | 1 | 23.79 |
| 7/5/2016 | | 1 | | | | | | | | | | 1 | 13.21 |
| 7/21/2016 | | 1 | | | | | | | | | | 1 | 22.03 |
| 7/21/2016 | | | | | 1 | | | | | | | 1 | 16.67 |
| 7/22/2016 | | | | | 1 | | | | | | | 1 | 4.65 |
| 7/29/2016 | | | 1 | | | | | | | | | 1 | 29.25 |
| 8/2/2016 | | | | | 1 | | | | | | | 1 | 5.64 |
| 8/22/2016 | | 1 | | | | | | | | | | 1 | 26.11 |
| 8/25/2016 | | | | | 1 | | | | | | | 1 | 18.74 |
| 9/2/2016 | | | | 1 | | | | | | | | 1 | 2.82 |
| 9/7/2016 | | 1 | | | | | | | | | | 1 | 4.68 |
| 9/23/2016 | | 1 | | | | | | | | | | 1 | 101.60 |
| 9/30/2016 | | | | | 1 | | | | | | | 1 | 2.76 |
| 10/1/2016 | | | 1 | | | | | | | | | 1 | 4.45 |
| 10/9/2016 | | 1 | | | | | | | | | | 1 | 1.57 |
| 10/11/2016 | | | | | 1 | | | | | | | 1 | 1.21 |
| 10/20/2016 | | | | | 1 | | | | | | | 1 | 3.36 |
| 11/2/2016 | | | 1 | | | | | | | | | 1 | 4.61 |
| 11/15/2016 | | | | | | | 1 | | | | | 1 | 2.54 |

| Date | Landsat l5 | Landsat l7 | Landsat l8 | Sentinel 1 | Sentinel 2 | ASTER | RADARSAT | TERRA SAR | world view | envisat | ers E2 | total | Area Km2 |
|---|---|---|---|---|---|---|---|---|---|---|---|---|---|
| 11/17/2016 | | | | | | | 1 | | | | | 1 | 36.42 |
| 12/28/2016 | | 1 | | | | | | | | | | 1 | 13.75 |
| 2/27/2017 | | | | 1 | | | | | | | | 1 | 0.18 |
| 3/23/2017 | | | | 1 | | | | | | | | 1 | 62.19 |
| 4/4/2017 | | | | 1 | | | | | | | | 1 | 2.86 |
| 4/16/2017 | | | | 1 | | | | | | | | 1 | 1.86 |
| 4/18/2017 | | | | | 1 | | | | | | | 1 | 10.27 |
| 4/25/2017 | | | | | | | 1 | | | | | 1 | 17.80 |
| 4/25/2017 | | | | | | | | 1 | | | | 1 | 8.30 |
| 4/28/2017 | | | | 1 | | | | | 1 | | | 1 | 60.29 |
| 6/3/2017 | | | | 1 | | | | | | | | 1 | 1.31 |
| 6/27/2017 | | | | 1 | | | | | | | | 1 | 19.33 |
| 7/9/2017 | | | | 1 | | | | | | | | 1 | 31.13 |
| 8/2/2017 | | | | 1 | | | | | | | | 1 | 12.97 |
| 8/14/2017 | | | | 1 | | | | | | | | 1 | 85.32 |
| 9/1/2017 | | | 1 | | | | | | | | | 1 | 7.75 |
| 9/1/2017 | | | | 1 | | | | | | | | | 29.63 |
| 9/7/2017 | | | | 1 | | | | | | | | 1 | 11.57 |
| 10/13/2018 | | | | 1 | | | | | | | | 1 | 28.14 |
| 10/19/2017 | | | 1 | | | | | | | | | 1 | 3.15 |
| 11/18/2017 | | | | 1 | | | | | | | | 1 | 82.20 |
| 11/30/2017 | | | | 1 | | | | | | | | 1 | 31.47 |
| 12/12/2017 | | | | 1 | | | | | | | | 1 | 2.61 |
| 12/24/2017 | | | | 1 | | | | | | | | 1 | 36.74 |
| 1/29/2018 | | | | 1 | | | | | | | | 1 | 8.45 |
| 2/10/2018 | | | | 1 | | | | | | | | 1 | 22.87 |
| 3/6/2018 | | | | 1 | | | | | | | | 1 | 62.22 |
| 3/18/2018 | | | | 1 | | | | | | | | 1 | 68.67 |
| 3/24/2018 | | | | | 1 | | | | | | | 1 | 5.93 |
| 4/13/2018 | | | 1 | | | | | | | | | 1 | 2.19 |
| 4/28/2018 | | | | | 2 | | | | | | | 2 | 96.60 |
| 4/29/2018 | | | 1 | | | | | | | | | 1 | 67.30 |
| 4/30/2018 | | | | | | 1 | | | | | | 1 | 1.62 |
| 5/5/2018 | | | | 1 | | | | | | | | 1 | 47.10 |
| 5/23/2018 | | | 1 | | | | | | | | | 1 | 116.81 |

| Date | Landsat l5 | Landsat l7 | Landsat l8 | Sentinel 1 | Sentinel 2 | ASTER | RADARSAT | TERRA SAR | world view | envisat | ers E2 | total | Area Km2 |
|---|---|---|---|---|---|---|---|---|---|---|---|---|---|
| 5/29/2018 | | | | 1 | | | | | | | | 1 | 4.87 |
| 5/31/2018 | | | 1 | | | | | | | | | 1 | 21.03 |
| 6/8/2018 | | 1 | | | | | | | | | | 1 | 12.18 |
| 6/16/2018 | | | 1 | | | | | | | | | 1 | 46.78 |
| 6/22/2018 | | | | 1 | | | | | | | | 1 | 48.05 |
| 6/24/2018 | | 1 | | | | | | | | | | 1 | 37.43 |
| 6/28/2018 | | | | 1 | | | | | | | | 1 | 11.29 |
| 7/4/2018 | | | | 1 | | | | | | | | 1 | 24.85 |
| 7/10/2018 | | 1 | | | | | | | | | | 1 | 4.01 |
| 7/15/2018 | | | | | | | 1 | | | | | 1 | 37.04 |
| 7/16/2018 | | | | 1 | | | | | | | | 1 | 68.02 |
| 7/20/2018 | | | | | | | 1 | | | | | 1 | 22.10 |
| 7/26/2018 | | 1 | | | | | | | | | | 1 | 35.52 |
| 8/3/2018 | | | | 1 | | | | | | | | 1 | 11.16 |
| 8/20/2018 | | | | | | | 1 | | | | | 1 | 52.48 |
| 8/21/2018 | | | | 1 | | | | | | | | 1 | 53.36 |
| total | 48 | 100 | 46 | 33 | 22 | 1 | 6 | 1 | 1 | 11 | 0 | 268 | |
| | | | | | | | | Average | | | | | 22.96 |

**3.5 OIL THICKNESSES ON AERIAL AND SATELLITE IMAGERY.**

The sun glint effect in optical remote sensing has been used to detect oil slicks on the ocean surface. The main factor that determines the thickness of an oil spill is the amount of oil and the rate of its discharge on the ocean surface. Generally, following initial surfacing, as crude oil spreads and the thickness reduces, it changes in appearance from the black or dark brown coloration of thick crude oil to iridescent and silver sheen in the thin layers at the edges of the slick. If those sheens then converge, the thickness of the oil can increase and the oil develops into a thicker emulsion that is created as a combination of the wave action, photo-oxidation, and evaporation. I have produced a number of videos for research/academic purposes over the MC20 site that explain these processes. Multiple videos for reference are listed on Appendix D.

Sheens consist of very thin films that are distinguishable because of the viscoelastic properties of the oil that retain surface tension on the water. The sheen forms a surface that reflects more of the light and can appear to be relatively brighter than the clean water surface depending on the viewing angle between the observer and the ambient light source. After spreading, the light volatile components of the crude oil begin to evaporate. The rate of evaporation depends upon the vapor pressure and the volatile components present in the crude oil. Furthermore, the remaining concentrated portion of crude oil mixes with the surface seawater under the influence of wind and wave action to form an emulsion. The material formed can be either a water-in-oil (w/o) or an oil-in-water (o/w) emulsion depending on what substance (water or oil) prevails more on the emulsion.

In 2004, ***the Bonn Agreement Oil Appearance Code (BAOAC)*** was adopted worldwide as a standard method to assess the volume of oil on water. This is the equivalent to the ASTM-F2534. A copy of these two can be found on Appendix E. According to the BAOAC handbook, the oil slick thickness is coded as: sheens (silver/gray), rainbow, metallic, discontinuous true oil color, and continuous true oil color. In 2016, NOAA and the U.S. Coast Guard released the Open Water Oil Identification Job Aid (OWOIJA) to describe oil slicks. This Job Aid is designed to describe oil slicks appearance for spill response operations and it uses the same thicknesses ranges of the BAOAC. In my opinion OWOIJA has been a very useful documentation that helps responders to easily understand the aspect of the different oil thicknesses. A copy of this OWOIJA can also be found on Appendix E.

As stated on the OWOIJA: "Oil thickness standards presented here are based on the Bonn Agreement Oil Appearance Code (BAOAC) and are more descriptive of the colors typically observed from aircraft. Other standards exist, such as ASTM F-2534-12, often used by industry personnel conducting overflights. These standards have become widely used and taught throughout the response community. In NOAA's experience, use of these standards promotes observational simplicity, consistency, and clearer communication in describing the appearance and structure of an oil slick. Therefore, NOAA continues to support and advocate the nomenclature, and codes presented in this Job Aid".

For illustration purposes, an aerial photograph collected over the MC20 area of leaked oil on May 2016 is shown in Figure 22 and 23. I will refer to BAOAC for the discussion of oil thicknesses, following the nomenclature that is based on their appearance as:

**S**) **Sheen,** as a layer of floating oil for which layers of different thickness vary in color from rainbows (for the thicker layers), to silver/gray (for the thinnest), to almost transparent.

**M) Metallic,** the next distinct oil color, thicker than rainbow, that tends to reflect the color of the sky, but with some element of oil color, often between a light gray and a dull brown.

**T) Transitional Dark** (or True) color: The next distinct oil on water layer thickness after metallic, which tends to reflect a transitional dark or true oil color.

**D) Dark** (or True) Color: Represents a continuous true oil color (i.e., its natural color), commonly occurring at thicknesses of at least a hundreds of micrometers.

This Figure 22 (source from the OWOIJA job aid page 12) captures the oil classes in a simple graphical way.

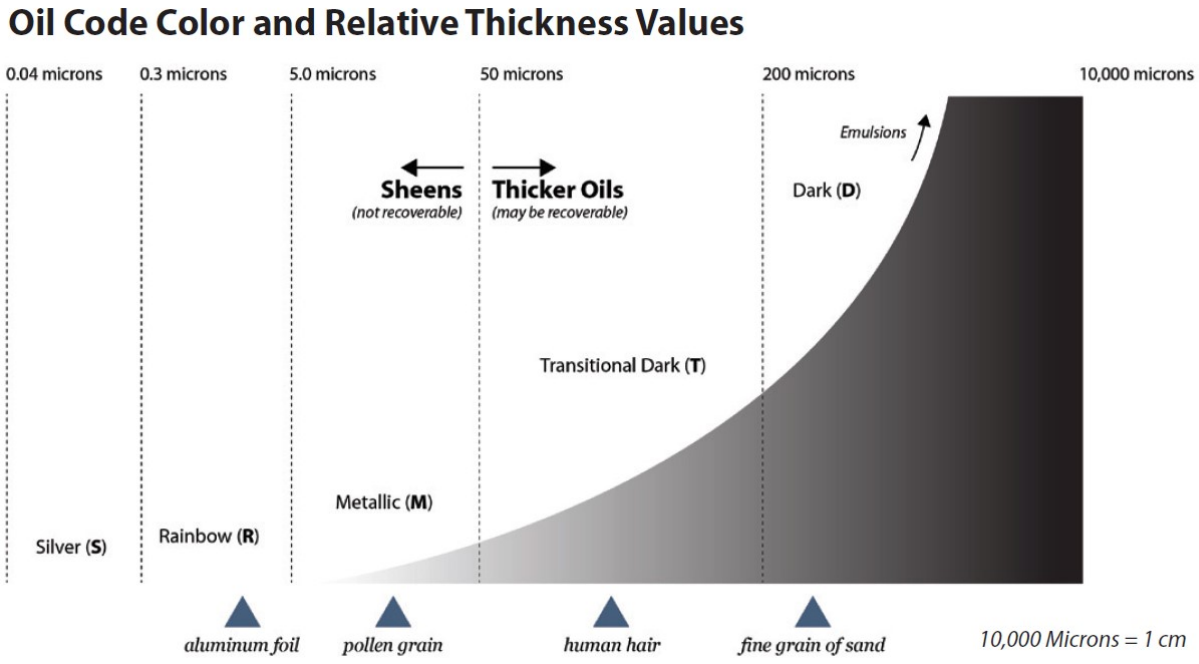


Figure 22. Oil thickness classes range.

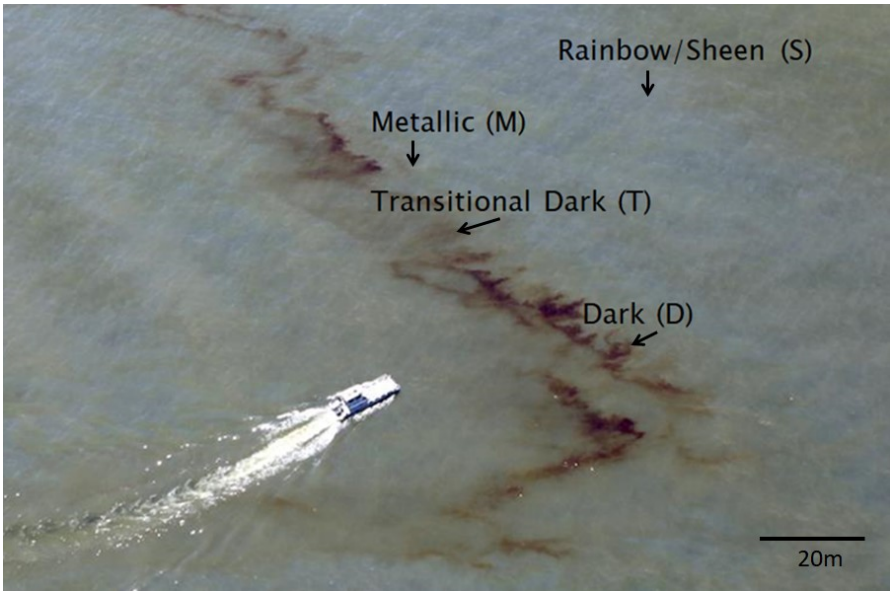


Figure 23 - Aerial photo of oil leakage around the MC20 lease block collected on May 8, 2016, during a research cruise. The location of the research vessel was 28.94N and 88.97W. Photo credit: B. Shumaker.

**3.6 OIL THICKNESS MEASUREMENTS**

Estimating the oil thickness based on the aspect of the floating oil is different than having a physical measurement. In addition to the assessment of the thickness based on its aspect or visual appearance (according to the BAOC), and in an attempt to validate the estimates given by the visual inspection, I have used three different techniques for physically measuring the oil thicknesses during experiments at OHMSETT and at the USF Optics Labs: 1) Absorbent pads, which were suitable for thin oils up to a few hundreds of microns thick; 2) dip plates, whose performance depends on the level of emulsification; and 3) the automated Water Mapping Oil Thickness Sampler (WM-OTS), which was demonstrated to measure oil thicknesses from 5 microns to several centimeters. I will focus the analysis on the results obtained using the WM-OTS, because of its consistency and broader range of operation.

The WM-OTS consists of a mechanical device that uses a glass tube of a 4.13 cm in diameter that collects, insofar as possible, an undisturbed depth profile of the floating surface oil. This is accomplished as follows: The tube is suspended on a floating mount that holds both the tube and a mechanism that caps the tube from both ends after the oil/water sample is inside the tube. Before the sample collection, the tube is treated with an oleophobic coating that allows the oil to enter the tube freely, without sticking to the walls. Once the tube is placed into the water on which floats a layer of oil, a floating sensor triggers a servo motor that caps the tube from under and above the water line. After the sample is collected, the exterior of the tube is cleaned and the tube is prepared for thickness measurement. The thickness of the oil (and its volume) is measured with high resolution digital photography and by extracting the oil/water sample with Toluene, which separates the oil from the water.

Calibration experiments of the WM-OTS have taken place at OHMSETT and at the USF. The calibration tests consisted on sampling controlled thicknesses with the WM-OTS so we could create a library of thicknesses for different oils. The concept behind this calibration is that known oil thicknesses of (40, 80, 120, 160, 200, 240, 280, 320, 360, 400, 600, 800 um) from different oil types were sampled with the WM-OTS to understand the thicknesses measured by a super high resolution camera (Figure 24).

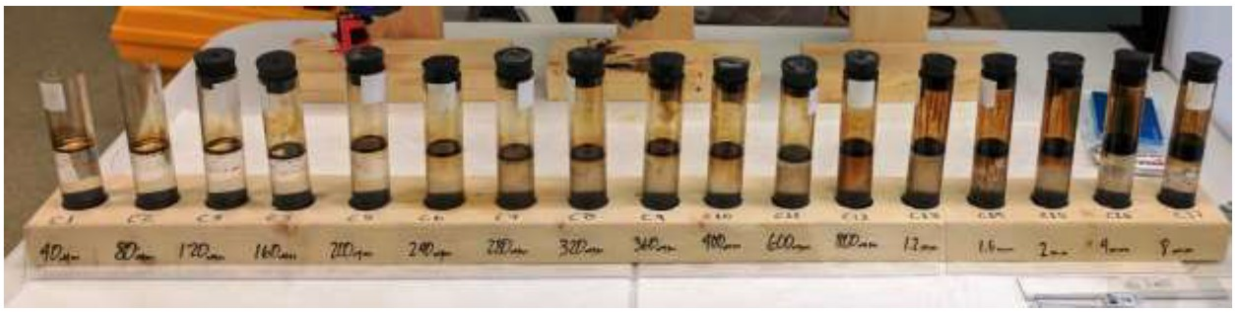

Figure 24. Examples of oil extracts collected by the WM-OTS oil sampler during a lab Experiment. Samples ranging from 40um to 8mm are shown here.

Once these calibration curves are collected, we can now relate samples collected on the field with their best match obtained on the lab (Figure 25).

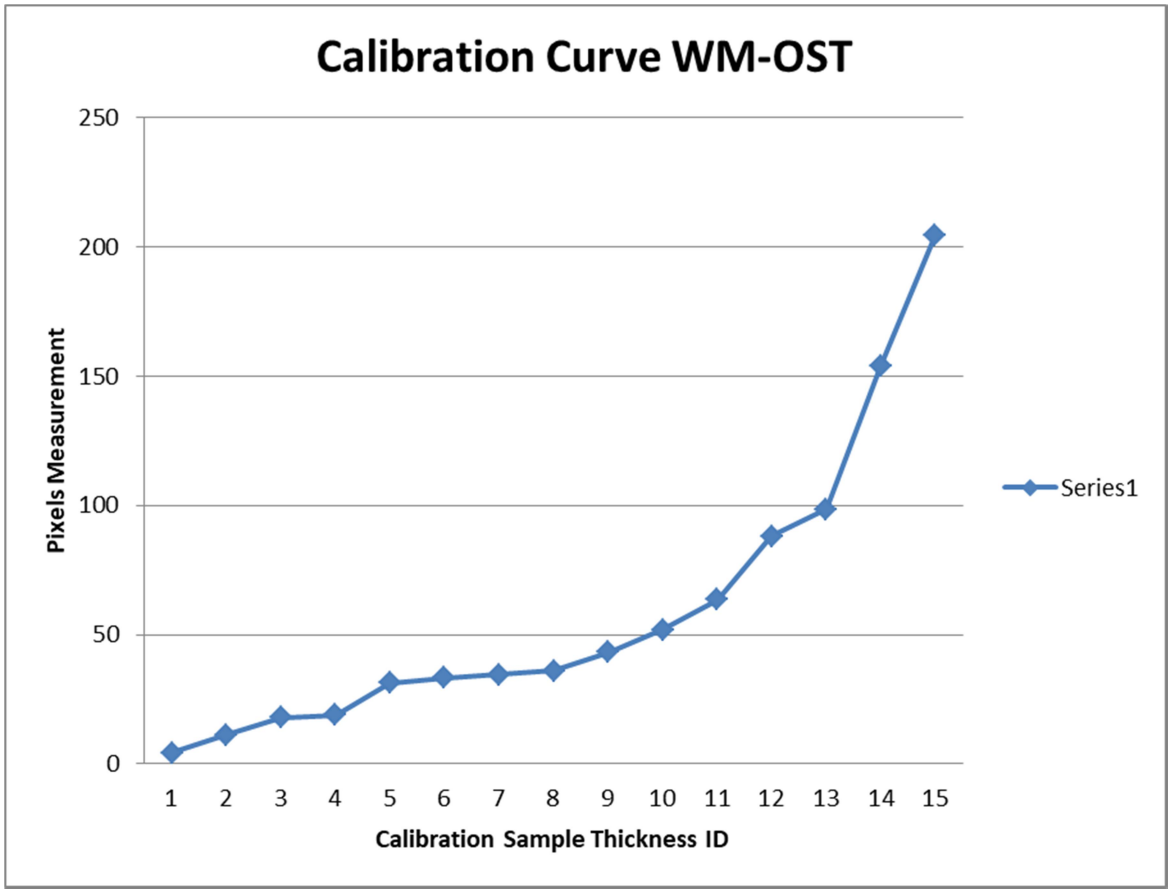


Figure 25 Calibration curve of oil thicknesses measurements with WM-OST

Having this calibration curve created from the tests on the lab (under controlled thicknesses) allows us to collect samples on the field and once the sample is processed (with the high resolution photography) we can obtain the thickness of the sample by relating the thickness in pixels from the photography, with its physical thickness in micrometers. Oil thickness measurements in the lab (OHMSETT, Water Mapping, and USF) ranged from 5µm to 2 cm. The calibration of WM-OST under this range covers all the samples that I have ever collected at MC20 site which have ranged from 15µm to 400µm (Figure 6).

Figure 6 - A): Photo of the floating emulsion from MC20 as it is sampled by the WM-OST. B): View of the sampler after being retrieved from the water. C): High resolution photo of the oil in the tube for which thickness was measured digitally at 80 µm. D): Area

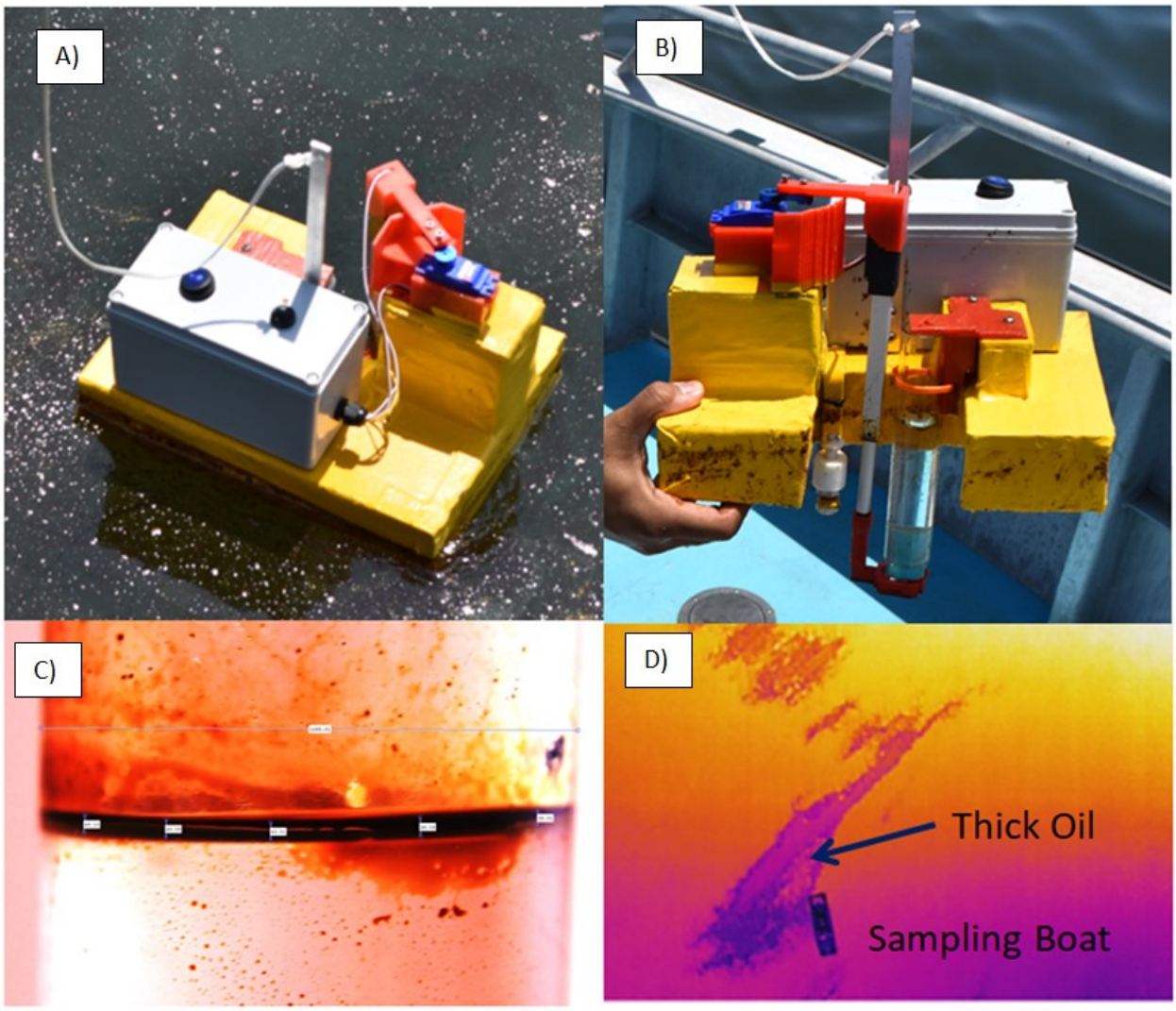


Thicknesses captured on the field are then compared to a calibration curve obtained on the lab. The way I use the sampler is in combination with UAS real-time imagery. I operate a UAS that broadcasts real time video on high definition (visual and thermal) to detect the thick patches of oil. Then I ask the captain of the vessel to position the boat in a tactical way so I (and the crew

that helps me) can collect samples and thickness measurements. Table 2 is an example of thickness measurements collected over the site, timing the collection with a satellite image.

Table 2 - Example of Oil Thickness Measurements

| WM-Tube | Date | Time Local (CT) | Waypoint | Lat (dd) | Long (dd) | Notes | Oil Thickness (microns) | Sample Picture | Area Photo | Area Photo2 |
|---|---|---|---|---|---|---|---|---|---|---|
| WM01 | 04/25/17 | 7:19:00 | 282 | 28.938774 | -88.964685 | Slick Description: Rainbow | 15 |  |  |  |
| WM02 | 04/25/17 | 7:28:00 | 286 | 28.939218 | -88.960496 | Slick Description: Rainbow | 15 |  |  |  |
| WM03 | 04/25/17 | 7:37:00 | 291 | 28.939479 | -88.956669 | Slick Description: Rainbow | 15 |  |  | |
| WM04 | 04/25/17 | 8:13:00 | 293 | 28.937308 | -88.960423 | Slick Description: Rainbow | 15 |  |  |  |
| WM05 | 04/25/17 | 12:06:00 | 320 | 28.940399 | -88.964097 | Slick Description: Thicker | 80 |  | 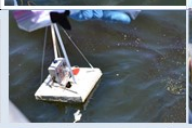 |  |
| WM06 | 04/25/17 | 12:11:00 | 322 | 28.94106 | -88.962643 | Slick Description: Thicker | 220 |  |  |  |
| WM09 | 04/25/17 | 12:14:00 | 324 | 28.941282 | -88.961985 | Slick Description: Thicker | 55 |  |  | |

As I mentioned earlier, the point of these measurements is to correlate these results with the satellite image to relate the sensor signal with the pixel values on the imagery. To achieve this correlation, the UAS photography is geo-referenced so we can identify the location of the samples with the features imaged by the drone.

Figure 27. Top: View from the UAS at the moment of a sample collection. Bottom: Photograph taken from the boat at the time of the sample collection.

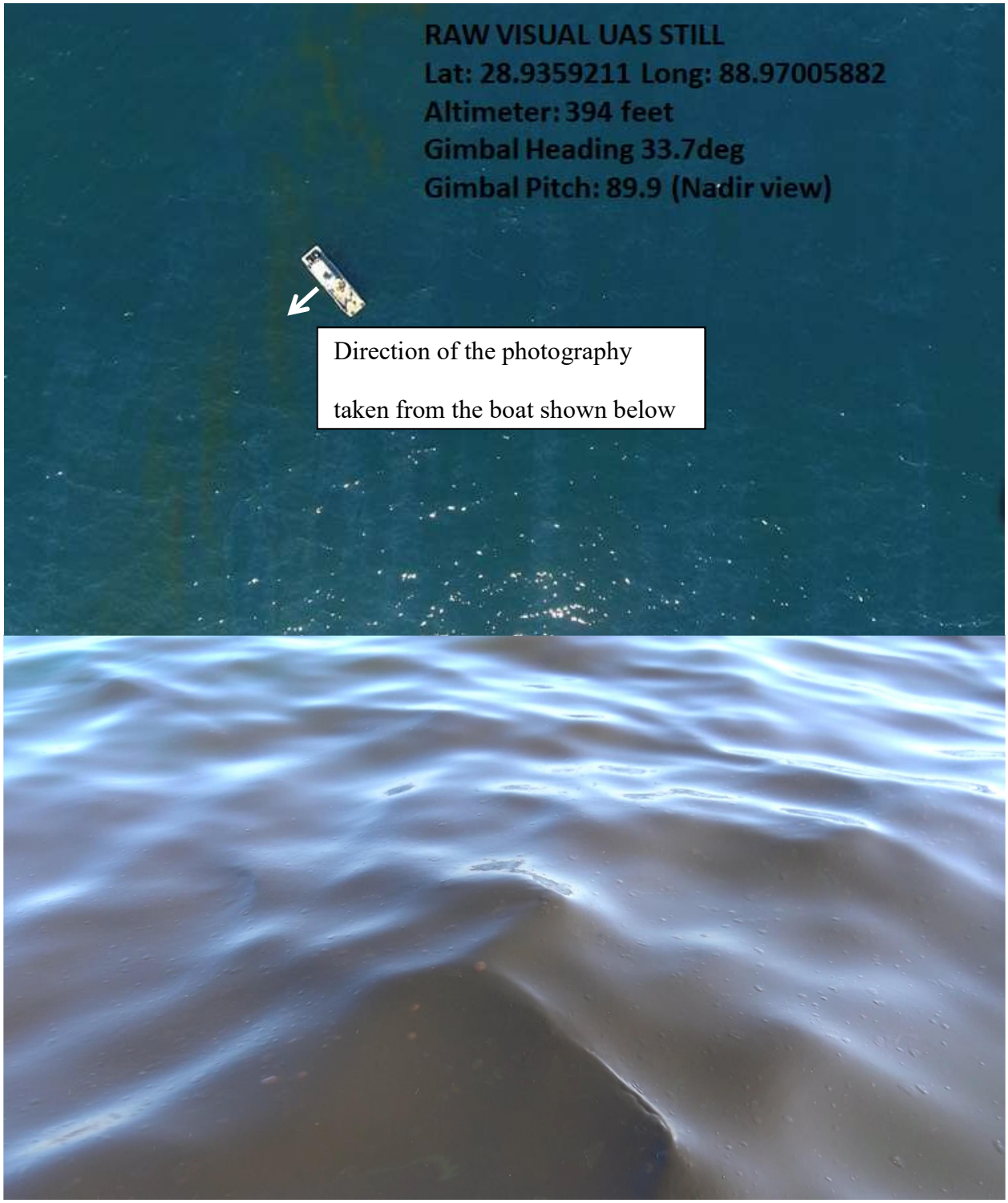

If one compares this photo on Figure 27-bottom with the one available on page 19 of the OWOIJA document on this appendix, one can clearly see the similarity of this patch with the Patch of Transitional (T) Color, which thickness falls between 50 to 200um. The WM-OST measurement on this patch was 180um. The Figure below is an example of how the thickness measurements are implemented into the satellite analysis and how the UAS was used to position the vessel on different areas of the slick. The basic concept behind this exercise is to use the physical measurements to validate our sea level and UAS observations so we can then apply these numbers into the satellite image classification.

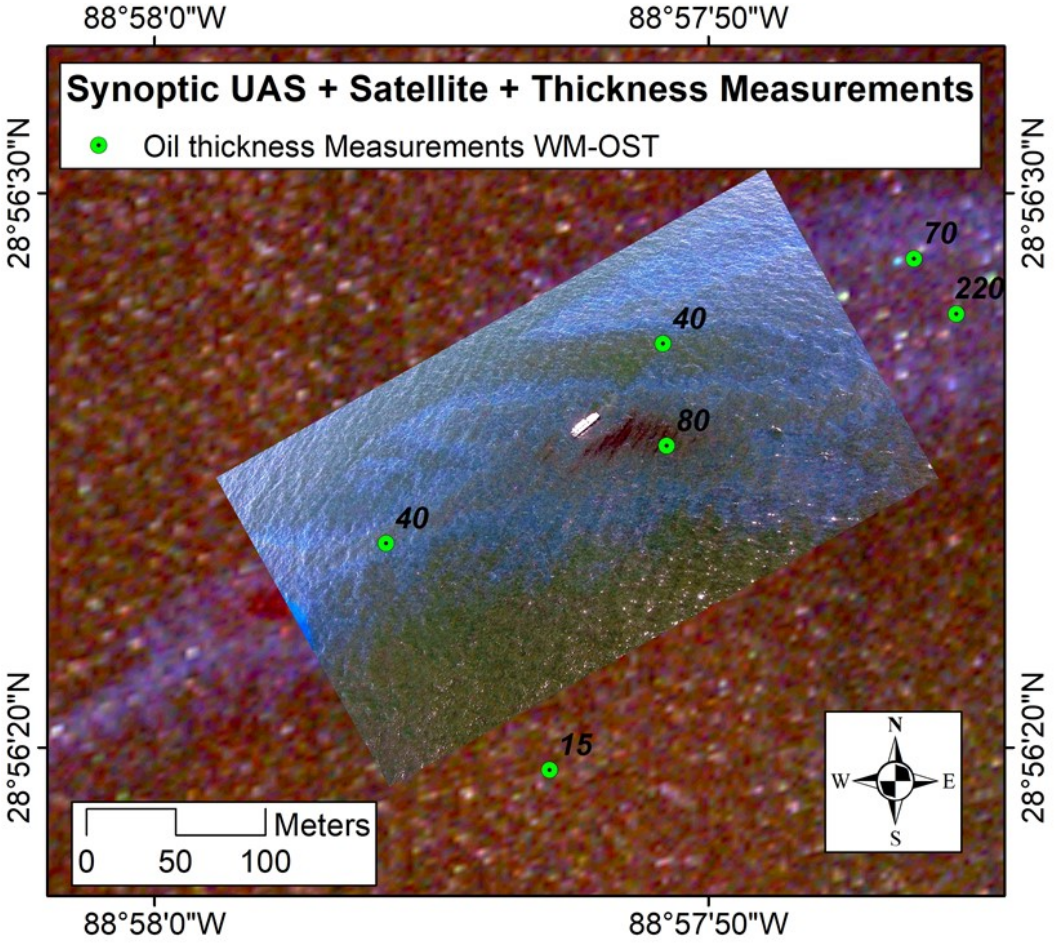


Figure 28 - Example of implementation of Thickness Measurements with Satellite Analysis. Green dots are sampling sites and their respective thicknesses in microns.

Figure  shows how those measurements are extrapolated into the entire satellite image. When these measurements are applied on the classification of the spectral signature of the entire satellite image, we can obtain 5 classes of thicknesses. These classifications were obtained using the image processing algorithms as published in [*Garcia-Pineda et al.*, 2012; *O Garcia-Pineda et al.*, 2017; *O Garcia-Pineda et al.*, 2013; *O Garcia-Pineda et al.*, 2009].

Figure 29 - Map of the MC20 slick with the 5 thickness classes. The classification areas resulted as 94% Sheen, 3.89% Rainbow, 1.12% Metallic, and 0.71% Dark Discontinuous, and 0.21% True color.

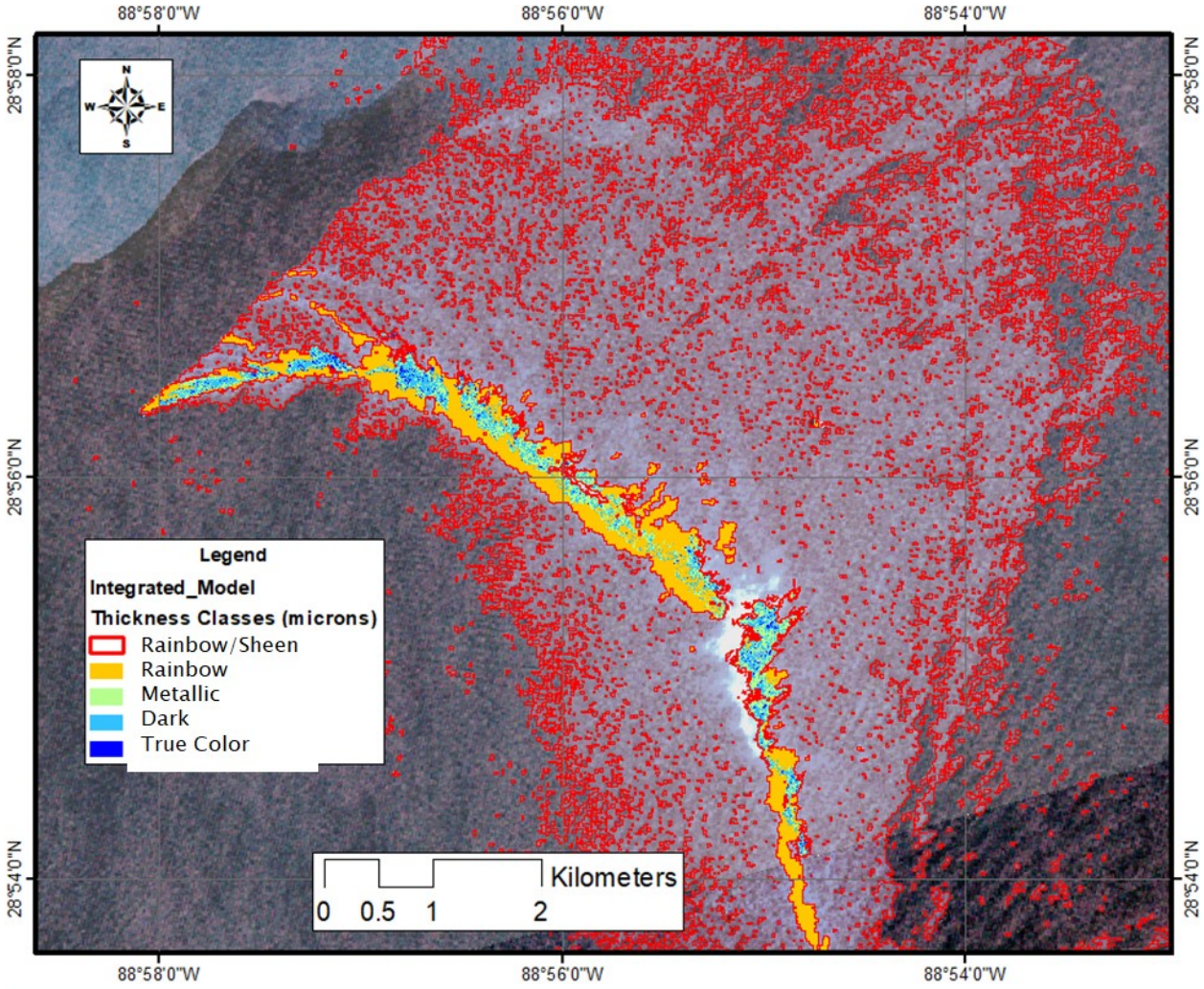

This Figure 30 shows a closer look to the level of detail on the classifications.

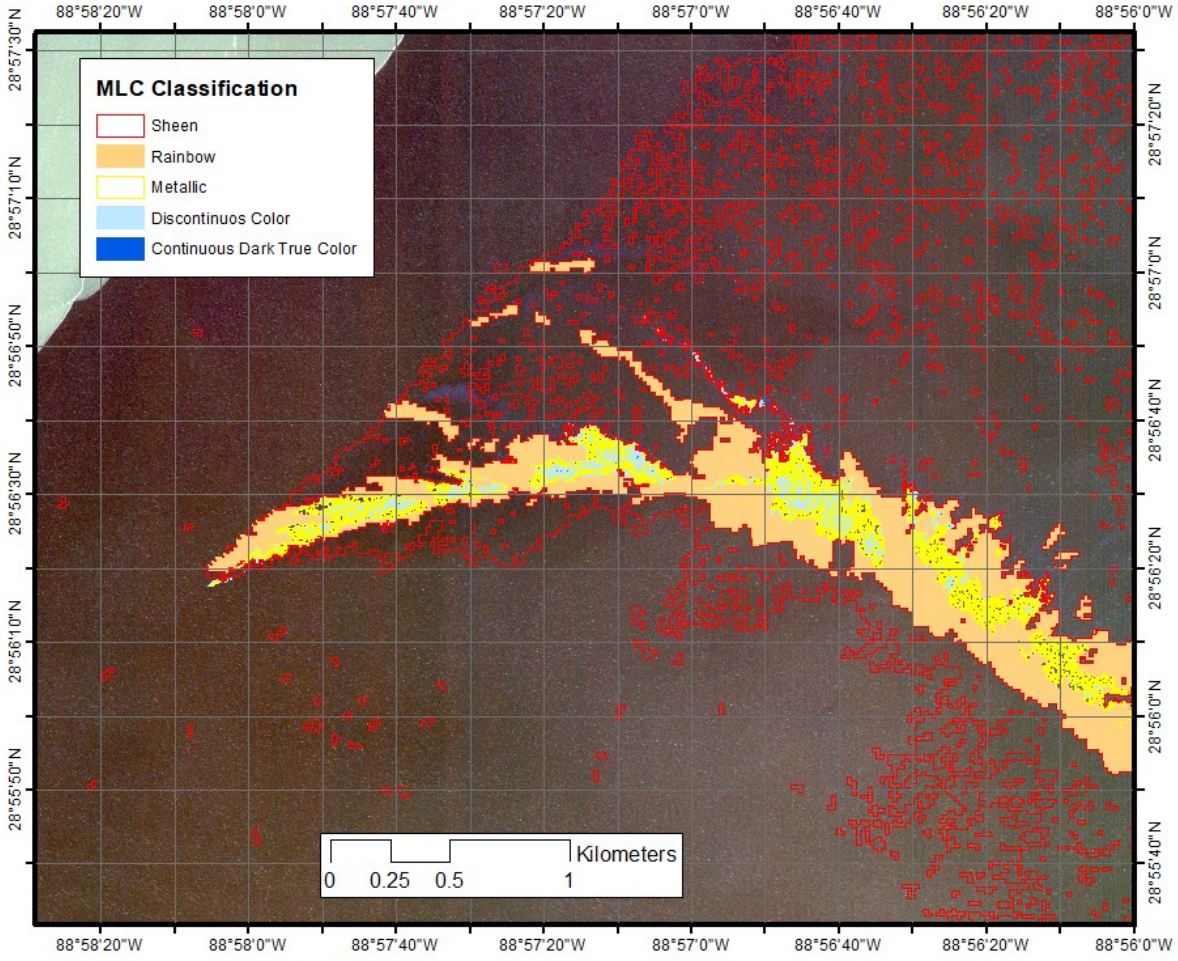


Figure 30 classifications made by the semi-automated image processing algorithm on a pixel by pixel basis. This is a supervised classification method that uses the processing routine known as Maximum-Likelihood-Classifier (MLC). The classification areas resulted as 94% Sheen (red outline), 3.89% Rainbow, 1.12% Metallic, and 0.71% Dark Discontinuous, and 0.21% True color.

There are 65 satellite images on the available dataset (collected after the last well intervention was complete on March 23, 2011) that showed the optimal reflectance conditions to at least classify the two main classes of oil. Table 3 is a list of the images which include the total area of the slick, the area classified as Thick, and the area classified as Thin. According to the BAOAC,

a THICK class that would include all thickness from 'Transitional Dark' and above (which would correspond to a layer of oil that conservatively would have from 50µm and above 200µm of thicknesses), and a second THIN class (which would contain the rainbow/sheens that would contain those layers related to rainbow/sheens in which thicknesses range would go from .04 µm to 50 µm).

Table 3 - Summary of Thickness Classifications in Satellite Images on chronological order after the completion of the last well decommission.

| Date | Oil Slick Extent | THIN | THICK | Percent |
|---|---|---|---|---|
| 3/25/2011 | 92.888 | 92.136 | 0.752 | 0.82 |
| 4/10/2011 | 20.824 | 18.127 | 2.696 | 14.87 |
| 4/18/2011 | 2.292 | 2.235 | 0.057 | 2.56 |
| 5/12/2011 | 35.065 | 34.731 | 0.334 | 0.96 |
| 5/20/2011 | 1.953 | 1.674 | 0.279 | 16.69 |
| 6/13/2011 | 138.900 | 136.692 | 2.207 | 1.61 |
| 6/29/2011 | 2.433 | 2.166 | 0.267 | 12.33 |
| 7/31/2011 | 3.124 | 2.928 | 0.197 | 6.71 |
| 8/24/2011 | 13.253 | 12.627 | 0.626 | 4.95 |
| 9/9/2011 | 31.288 | 30.599 | 0.689 | 2.25 |
| 4/21/2012 | 51.666 | 50.612 | 1.054 | 2.08 |
| 5/23/2012 | 11.699 | 10.781 | 0.918 | 8.52 |
| 6/8/2012 | 106.909 | 106.283 | 0.626 | 0.59 |
| 7/26/2012 | 2.460 | 2.239 | 0.221 | 9.89 |
| 8/11/2012 | 5.758 | 4.995 | 0.763 | 15.28 |
| 8/27/2012 | 9.009 | 8.720 | 0.288 | 3.31 |
| 9/28/2012 | 35.475 | 35.080 | 0.395 | 1.13 |
| 4/7/2013 | 19.942 | 19.303 | 0.638 | 3.31 |
| 4/23/2013 | 3.484 | 3.384 | 0.100 | 2.96 |
| 5/1/2013 | 2.902 | 2.775 | 0.127 | 4.59 |
| 5/9/2013 | 6.269 | 5.596 | 0.673 | 12.02 |
| 5/17/2013 | 9.831 | 8.624 | 1.207 | 14.00 |
| 5/25/2013 | 7.133 | 6.884 | 0.249 | 3.61 |
| 6/18/2013 | 34.758 | 33.065 | 1.693 | 5.12 |
| 8/5/2013 | 33.028 | 32.199 | 0.829 | 2.58 |
| 8/13/2013 | 10.276 | 9.882 | 0.394 | 3.99 |
| 8/21/2013 | 25.538 | 25.244 | 0.295 | 1.17 |

| Date | Oil Slick Extent | THIN | THICK | Percent |
|---|---|---|---|---|
| 1/12/2014 | 16.912 | 16.558 | 0.354 | 2.14 |
| 4/26/2014 | 93.355 | 90.205 | 3.149 | 3.49 |
| 5/4/2014 | 20.209 | 18.560 | 1.650 | 8.89 |
| 5/20/2014 | 30.827 | 27.344 | 3.483 | 12.74 |
| 6/21/2014 | 44.601 | 42.175 | 2.426 | 5.75 |
| 6/29/2014 | 50.171 | 48.598 | 1.572 | 3.24 |
| 10/27/2014 | 22.609 | 22.294 | 0.315 | 1.41 |
| 3/20/2015 | 14.980 | 14.707 | 0.273 | 1.86 |
| 3/28/2015 | 8.072 | 7.694 | 0.377 | 4.90 |
| 5/7/2015 | 15.248 | 14.600 | 0.648 | 4.44 |
| 5/31/2015 | 28.951 | 25.231 | 3.720 | 14.74 |
| 6/8/2015 | 58.552 | 57.746 | 0.805 | 1.39 |
| 6/24/2015 | 49.690 | 47.227 | 2.463 | 5.21 |
| 7/10/2015 | 102.328 | 100.263 | 2.065 | 2.06 |
| 9/20/2015 | 37.330 | 33.679 | 3.652 | 10.84 |
| 12/25/2015 | 5.814 | 5.625 | 0.189 | 3.36 |
| 4/8/2016 | 9.032 | 8.666 | 0.365 | 4.22 |
| 4/23/2016 | 39.086 | 38.046 | 1.040 | 2.73 |
| 4/24/2016 | 35.974 | 33.315 | 2.659 | 7.98 |
| 5/14/2016 | 2.188 | 1.680 | 0.508 | 30.22 |
| 5/23/2016 | 2.856 | 2.550 | 0.306 | 12.00 |
| 5/26/2016 | 8.407 | 7.999 | 0.408 | 5.10 |
| 6/3/2016 | 120.617 | 118.885 | 1.732 | 1.46 |
| 6/23/2016 | 32.578 | 31.646 | 0.932 | 2.95 |
| 7/21/2016 | 22.033 | 19.753 | 2.279 | 11.54 |
| 7/29/2016 | 29.246 | 28.047 | 1.199 | 4.27 |
| 8/25/2016 | 18.739 | 16.588 | 2.151 | 12.97 |
| 9/23/2016 | 101.599 | 99.500 | 2.100 | 2.11 |
| 9/30/2016 | 2.756 | 2.416 | 0.340 | 14.07 |
| 10/1/2016 | 4.447 | 4.131 | 0.316 | 7.66 |
| 4/18/2017 | 10.266 | 7.336 | 2.930 | 39.94 |
| 3/24/2018 | 5.927 | 5.612 | 0.316 | 5.63 |
| 4/29/2018 | 67.297 | 60.103 | 7.195 | 11.97 |
| 5/23/2018 | 116.807 | 110.521 | 6.286 | 5.69 |
| 5/31/2018 | 21.035 | 18.047 | 2.988 | 16.55 |
| 6/16/2018 | 46.775 | 40.526 | 6.249 | 15.42 |
| 6/24/2018 | 37.435 | 32.734 | 4.700 | 14.36 |
| Average | 32.08 | 30.63 | 1.45 | 7.39 |

The BAOAC states on Point 7.7 that a general rule is that 10% of the slick would contain the thicker oil (see Appendix E-BONN Agreement). One important result from this analysis is that, of the 65 images we analyzed we found an average of 7.39% of the area would correspond to a THICK class. Therefore using this approach for further calculations would be more conservative than using the 10% suggested by the BAOAC approach.

The results shown on table 4 means that in average, 92.61% of the oil areas produced by MC20 in the satellite imagery corresponded to thin oil, and 7.39% of the areas would correspond to thick oil. This result is consistent with the classification obtained by the high resolution imagery presented on Figure 29 (94% Sheen, 3.89% Rainbow, 1.12% Metallic, and 0.71% Dark Discontinuous, and 0.21% True color) using high resolution satellite imagery. From these three approaches the most conservative is the result obtained by the highest resolution imagery due to its ability to capture features at the highest possible level (90% Thin oil used by the general rule cited on the Bonn agreement, versus 92.61% Thin oil calculated from 65 optical images, versus 94% calculated from super high resolution imagery). Using the results obtained by the highest resolution imagery would generate the lower estimate on the volume calculations because smaller areas will be assigned to the thickest oil classes.

**3.7 VOLUME CALCULATIONS BASED ON INDUSTRY STANDARS.**

In order to measure volume of any feature, one needs to multiply an area by a given thickness. As an example to explain the volume measurement methodology, a simple calculation would be to assume a single thickness across the entire extent of an imaginary slick. For example, if we assign conservative rough estimate value of 1 μm across the entire extent of the slick, and we

consider an imaginary slick of 1 $km^2$ the following formula allows for a simple conversion of the area of a slick into volume measurement:

$1km^2$ x 1µm= $1m^3$ (or equivalent to 6.3 Barrels or 280 gallons of oil).

The three methods cited on this report: Bonn Agreement (BAOAC), NOAA-OWOIJA, and ASTM-F2534 (included on Appendix E) are widely used as standards to assess oil spills. The three standards use similar ranges of thickness for the evaluation of the oil spills, which are based on the physical process of the electromagnetic spectrum interacting with the floating oil. BAOAC is adopted in Belgium, Denmark, France, Germany, Ireland, The Netherlands, Norway, Sweden, and England (see page 6 on the aerial operational handbook of the Bonn Agreement). The oldest of these methods is the ASTM (which includes averages from observations made from 1930 to 2003), then the Bonn Agreement (established in 2004 and updated in 2016), and finally OWOIJA published in 2016 (which ranges are identical to those adopted by Bonn Agreement). So for my analysis I will use the Bonn Agreement Oil Appearance Code.

***Thickness Band for Allocated Appearance***

| | |
|---|---|
| Sheen | 0.04 µm – 0.3 µm |
| Rainbow | 0.3 µm – 5.0µm |
| Metallic | 5.0 µm – 50 µm |
| Dark | 50 µm – 200 µm |
| True Color | More than 200 µm |

Using the ranges defined above, we would obtain two results for the volume estimation, a minimum and a maximum estimate. According to the most conservative measurement of the

classes of oil observed on the MC20, I will use the percentages obtained by the high resolution imagery classification as shown on the Table 5 below.

Table 5. Percentage of oil classes per area for oil volume calculation

| | |
|---|---|
| Sheen | 94% |
| Rainbow | 3.89% |
| Metallic | 1.12% |
| Dark Discontinuous Color | 0.71% |
| True Color | 0.21% |

Although we can obtain a minimum and maximum estimate for each of the satellite images, the objective of this exercise is to understand a flow rate over time, thus, looking into individual snapshots would not be appropriate. Accordingly, I considered it necessary to use the average of multiple images over time. If used the average from only the high resolution multispectral imagery (Table 4), then the average would be 32.08 $km^2$. However, I did use the overall average obtained from all the satellite observations (Including SAR and Optical from table 2) over MC20 after the wells were decommissioned in March of 2011. This average is of 22.56 $km^2$ (equivalent to 8.7 square miles).

Using the Average area of 22.56km2 we can now estimate a minimum and a maximum volume of oil observed by the satellites. This is done by converting the areas of the slicks detected on the satellites into a range of minimum-maximum volume of oil. I will follow the exact same volume estimation procedure as described by the Bonn Agreement (as shown on Appendix B/BAOAC-page 16).

***Minimum Volume Calculation***

Using the average of 22.56 for the estimation of the minimum volume, the calculation would be:

Oiled Area x Area Covered with Specific Appearance x Minimum Thickness

Appearance 1 (Sheen)

22.56 $km^2$ x 94% x 0.04 µm = 0.85 $m^3$

Appearance 2 (Rainbow)

22.56 $km^2$ x 3.89% x 0.3 µm = 0.26 $m^3$

Appearance 3 (Metallic)

22.56 $km^2$ x 1.12% x 5.0 µm = 1.26 $m^3$

Appearance 4 (Discontinuous Colour)

22.56 $km^2$ x 0.71% x 5.0 µm = 8.01 $m^3$

Appearance 5 (True Colour)

22.56 $km^2$ x 0.21% x 200 µm = 9.48 $m^3$

**Minimum Volume = 0.85 + .26 + 1.26 + 8.01 + 9.48 = 19.86$m^3$ (equivalent to 124.31 Barrels, or 5246 Gallons of oil)**

***Maximum Volume Calculation***

Using the average of 22.56 for the estimation of the maximum volume, the calculation would be:

Oiled Area x Area Covered with Specific Appearance x Maximum Thickness

Appearance 1 (Sheen)

22.56 $km^2$ x 94% x 0.3 µm = 6.36 $m^3$

Appearance 2 (Rainbow)

22.56 $km^2$ x 3.89% x 5 µm = 4.39 $m^3$

Appearance 3 (Metallic)

22.56 $km^2$ x 1.12% x 50 µm = 12.63 $m^3$

Appearance 4 (Discontinuous Colour)

22.56 $km^2$ x 0.71% x 50 µm = 32.04 $m^3$

Appearance 5 (True Colour)

22.56 $km^2$ x 0.21% x (more than) > 200 µm = > 9.48 $m^3$

**Maximum Volume = 6.36 + 4.39+ 12.63 +32.04+ > 9.48 = > 55.42 $m^3$ (equivalent to 348 Barrels or 11919 Gallons of oil).**

**3.8 OIL RESIDENT TIME**

A satellite image captures the presence of oil on a snapshot; in order to understand the volume of the flux, however, it is necessary to analyze the rate of the discharge as a measure of volume per time. There has been several studies aimed to understand the resident time (or life time) of floating oil on the ocean using different types of modeling and simulation computer programs [*Daneshgar et al.*, 2016; *MacDonald et al.*, 2015]. One alternative way to measure the life time of the floating oil would be to monitor its displacement as it is being transported by surface currents to see how long it lasts on the surface. In order to do this, I used drifters, which are GPS tracking devices developed specifically to track oil spills and surface currents. These instruments have been used in the past to understand the processes related to the transport of floating oil on the ocean. *Igor et al.*, (2012) and *Rohrs et al* (2012) used results obtained from in-situ observations and drifters deployments to improve the performance of oil transport models. *Jones*, (2016) reported how they used drifters to monitor and follow oil released on a controlled experiment in the North Sea. Other studies that used drifter experiments in relation to oil spills that were conducted in the GoM in the past include *Liu et al.*, (2013); *Reed et al.*, (1994).

In a recent study that I have participated in with colleagues from University of Miami through the Gulf of Mexico Research Consortium (GOMRI), we used drifters at the MC20 site as a natural laboratory to understand the possible pathways that oil could experience under different environmental conditions. Results of this study were recently published on a scientific article that I co-authored (*Androulidakes et al,* 2017). In this paper we report the high influence that river induced fronts have on the transport of the floating oil from MC20 (see video https://www.youtube.com/watch?v=T6X2HAsYPu8). Based on the results obtained from this

study and the outstanding performance of the drifters following the oil paths, I was motivated to use drifters to measure the residence time that oil could last floating on the surface, therefore, in order to determine how long oil from MC20 last on the surface, I carried out 6 drifter deployment experiments under different oceanographic and meteorological scenarios using multiple drifters each time.

In total, I deployed 16 GPS-Tracked drifters from research vessels within the MC20 site study area (approximately at 88.978W, 28.938N). I employed two classes of drifters (drogued and un-drogued), as we wanted to follow surface material pathways (floating oil) and distinguish it from possible subsurface (0.5 m below surface) material pathways (like oil droplets suspended in the upper meter). By using these two classes of instruments, we could examine if the presence (absence) of drifter drogue had an impact on following subsurface (surface) transport of oil. We assume that the river plume is deeper than the drogue depth and, therefore, the drogued drifters are also influenced by the plume and the respective density fronts. The drifters used on this study are described next:

**Drifter Type 1. CARTHE Un-drogued**

This is a low cost, biodegradable instrument that tracks oil by transmitting its position every 5 minutes. Figure 31 shows the CARTHE Un-drogued being held by my colleague Dr Lisa DiPinto (NOAA) as I am preparing the UAS before deployment at the slick source of MC20 site. More information about this drifter can be found here: http://carthe.org/

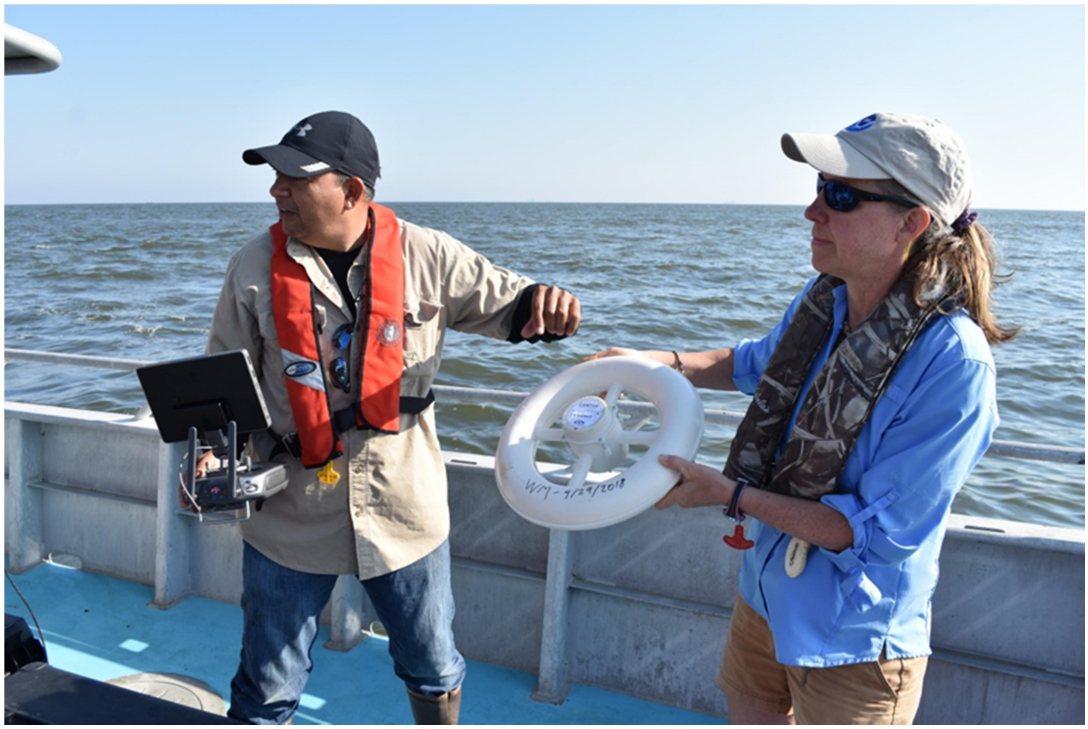

Figure 31- Dr. DiPinto holding the drifter before deployment, as it will be monitored by a UAS.

**Drifter Type 2. CARTHE Drogued**

The CARTHE Drogued drifter is the same instrument than the CARTHE Un-drogued, but it has two plates attached that function as a drag for the drifter. These plates (Figure 32) make the drifter to behave as subsurface currents (about 2 feet below surface), in contrast to the un-drogued drifter which behaves like top surface currents.

Figure 32. Drogued CARTHE drifter.

**Drifter Type 3. Met-Ocean Isphere**

The iSPHERE (Figure 33) is an expendable, low cost, bi-directional spherical drifting buoy. I deployed this drifter at the MC20 slick source site on three different ocassions. As described on iSPHERE website: *"The drifter was developed to meet the demanding needs of the offshore oil industry, ocean freight industry and the oceanographic scientific community. The buoy was designed specifically to track and monitor oil spill incidences"*. The iSPHERE drifter also provides real-time sea surface temperature data and GPS positional data. More information about this drifter can be found at https://www.metocean.com/product/isphere/ .

Figure 33. Isphere Drifter used on 3 deployments at the MC20 site.

**Drifter Type 4.**

The CODE/DAVIS drifter has been designed and tested to meet the performance criteria of the CODE (Coastal Ocean Dynamics Experiment) drifter developed by Dr. Russ Davis of SIO. I used and deployed this drifter at the MC20 slick source site on three different ocassions. The CODE/DAVIS drifter is designed to acquire coastal and esturarian water currents within a meter of the water surface. The CODE/DAVIS drifter is equipped with a sea surface temperature sensor, GPS receiver and the option of either Iridium® or ARGOS based satellite telemetry. For more information see https://www.metocean.com/product/codedavis-drifter/.

Figure 34 CODE Drifter. Photo source www.metocean.com

**Measuring Oil Resident Time with Drifters: Experiments design**

The experiments consisted of deploying different types of drifters at approximately the same time on the same place. I used a UAS to position the boat right at the source of the oil slick at MC20 and then my colleagues assisted me in deploying the drifters while I was observing the vessel on the UAS (see Figure 35). The objective was to track the drifters to measure how long it takes to be transported the same distance as the oil slicks. These deployments were scheduled to coincide with planned acquisitions of a variety of satellite images. I planned these missions at the MC20 site, monitoring weather and forecast models that allowed me to capture the displacement of the oil under different conditions, including under different wind/current directions and speeds.

Next I present the observations made during the six deployments where multiple satellite images captured this process.

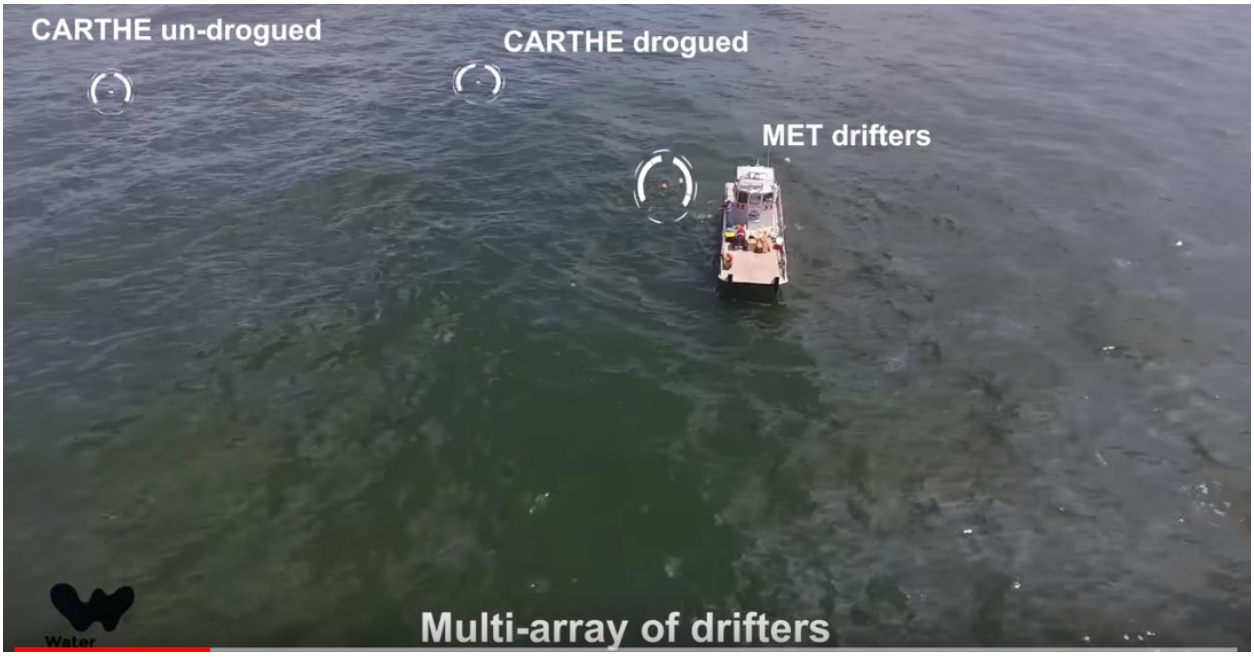


Figure 35. Deployment and monitoring of drifters with UAS.

**Case 1. April 20, 2017.**

A total of four drifters were deployed on this first experiment. The satellite image shown on Figure 36 shows the length of the trajectory of the oil slick and the trajectory of the drifters. On this deployment, drifters were influenced by easterly wind-induced surface currents and had trajectories along the Mississippi River front by the downstream current toward the west. The prevailing southeasterly winds between 20 and 22 April (Figure 36) determined this pathway, driving the surface waters along the outer plume front and finally toward the coast, west of the Louisiana Peninsula. It is noted that all undrogued drifters deployed on 18 and 20 April propagated westward along the front and their fate was largely determined by the extension of the plume and thus the front's location under the effect of strong easterly winds. The total length

of the slick was 24.5Km. The time that it took the un-drogged drifters to be displaced this distance was 10 hours.

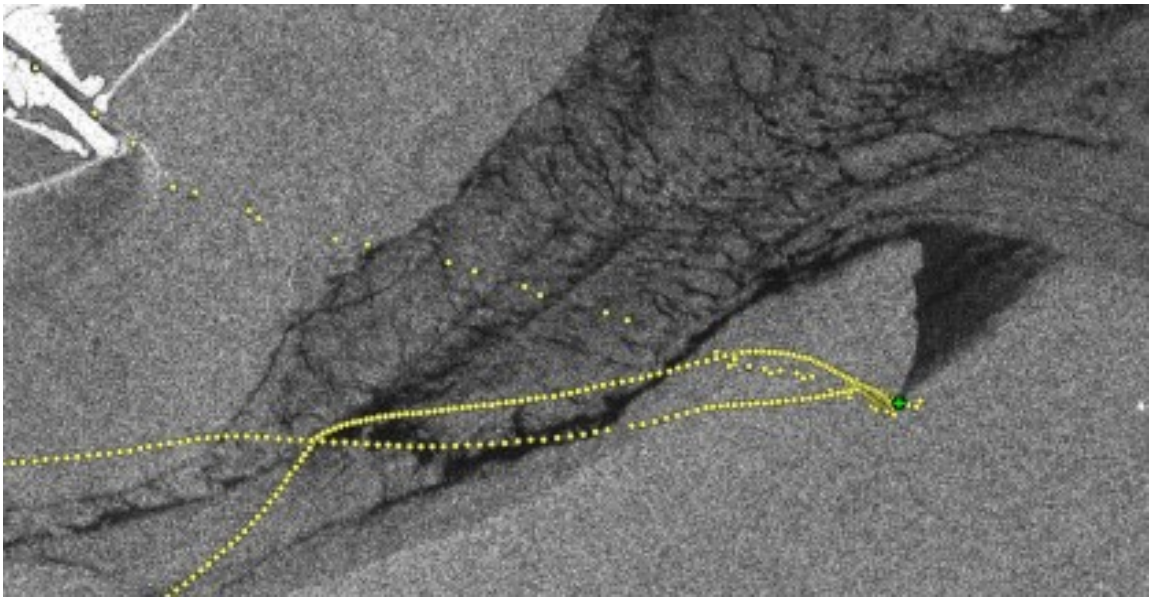

Figure 35. Satellite image obtained by SAR satellite RADARSAT just few minutes before the deployment of the drifters.

It is important to understand that the satellite image occurs in a snapshot, while the trajectory of the drifters is captured over a long period of time (several hours). This analysis uses the satellite image as a guide to see the length of the slick, and then uses the records from the drifter to estimate the time that it took the oil to travel that distance. It is expected that the shape of the slick captured on the satellite image will not match perfectly the trajectory of the drifters, but it should follow a similar directional pattern. For example, this satellite image, captured by RADARSAT approximately 1 hour before the deployment, shows the oil traveling almost straight north, however, then almost immediately after, the deployment shifted towards the west. Altough the trayectories are not identical, what is most important to watch is the wind strength before, during, and after the deployment.

The wind conditions before and after can be seen on the plot on Figure 36. These plots are records from 2 meteorological stations (SPLL1 and NDBC 42012) nearby the MC20 site and from two wind models (ECMWF and NAVGEM) showing the direction and magnitude of the wind prior to the satellite snapshot. This is an important observation because this wind history was the main factor driving and evaporating the oil slick as it appears on the satellite image. There is high consistency in the wind observations from the different platforms. The average wind speed during 10 hours before the time of the satellite snapshot was 6.23 m/s.

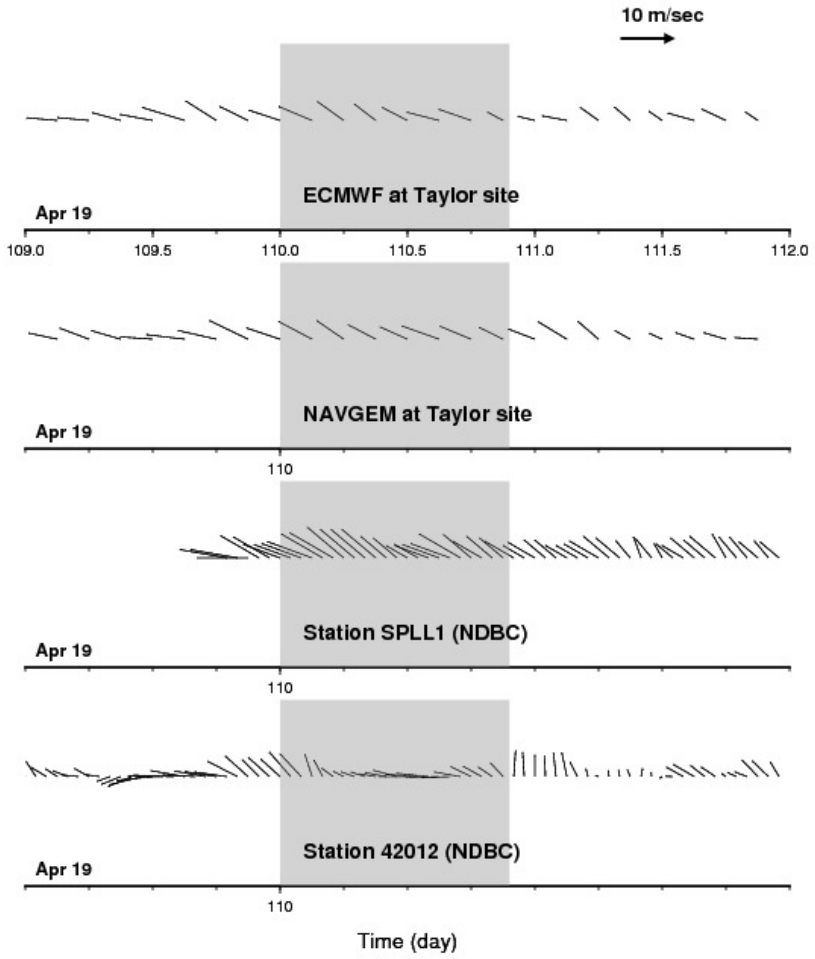


Figure 36. Wind direction and speed plots from 2 wind models and 2 nearby monitoring stations. The average wind speed over 10 hours before the deployment was 6.23m/s.

**Case 2. April 25, 2017.**

Two drifters were deployed on April 25, 2017. The drifters initially propagated eastward and then southward (Figure 37), following the dominant direction of the winds.

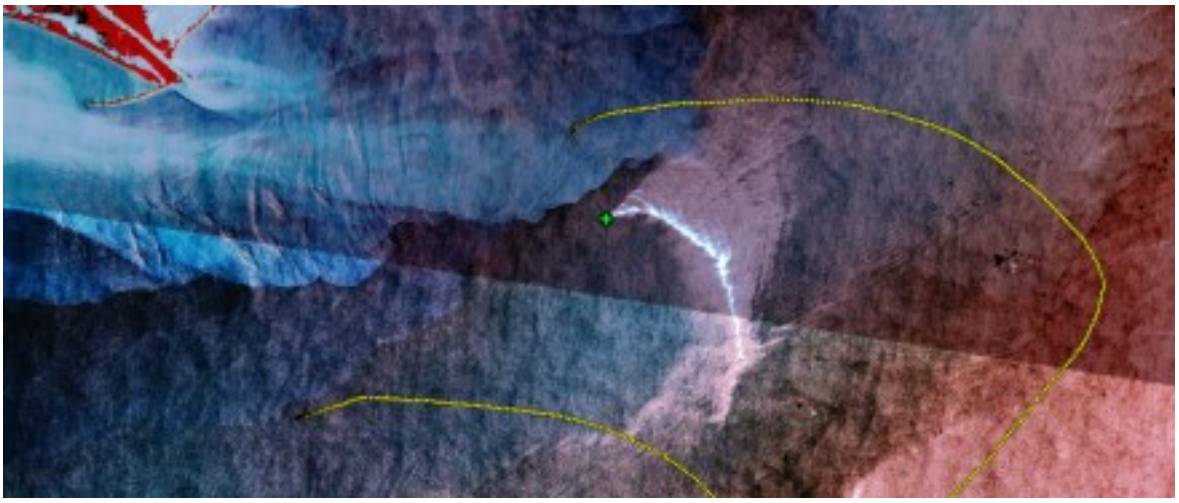

Figure 37. Drifter Deployments on April 25. The length of the slick was 13.6 miles and the time that took the drifters to travel that distance was 8 hours. The average wind speeds during that period of time was 9.12 m/s.

**Case 3, April 26, 2018**

Deployments on April 26 presented a unique opportunity due to the stronger winds that occurred that day. I am going to refer to this case as the "Strong Winds Case." Four drifter deployments occurred at the same time right at the location of the oil slick source. A satellite image collected by TerraSAR-X shows the displacement of the drifters in reference to the slick (Figure 38).

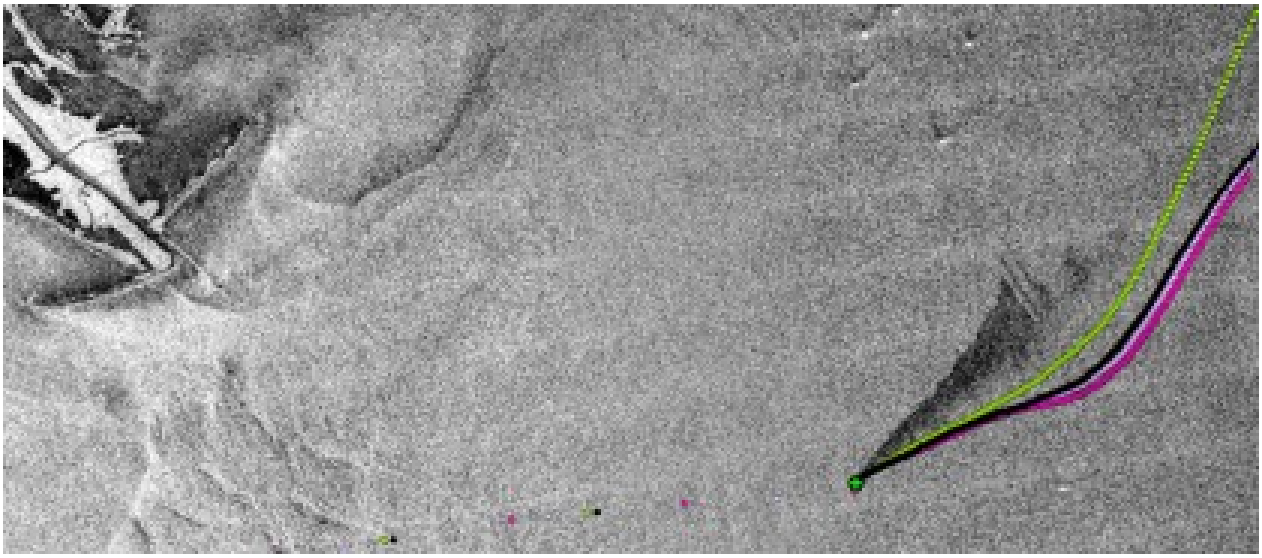

Figure 38. The length of the slick was 8.9km and the time that the drifters took to be displaced this distance was 6 hours. The average wind conditions during that period of time were 10.1 m/s.

**Case 4. August 16, 2017.**

In contrast to the previous case, on August 16, 2017 we experience very calm wind conditions for a long period of time. This will be the "Calm Wind Case." The length of the slick was of 54 km (Figure 39), the time that took drifters to travel this distance was 17 hours and the average wind speed was of 3m/s during that period of time. Despite the calm wind conditions, we observed very strong currents being produced by the extended river plume. A UAS video of the conditions of the slick observed this day can be seen here: https://youtu.be/0Ly0ktQbtCw

Figure 39. Image collected by CosmoSkymed showing a slick of 54km and the drifter trajectories.

**Case 5. April 29, 2018.**

Earlier this year, a fifth drifter deployment was carried out, during which I was able to drift with the oil for 6 continuous hours. I was able to confirm that the drifter not only followed the path of the oil, but stayed within the thick patch of oil at all times during the period of the time I followed (red dots on Figure 40).

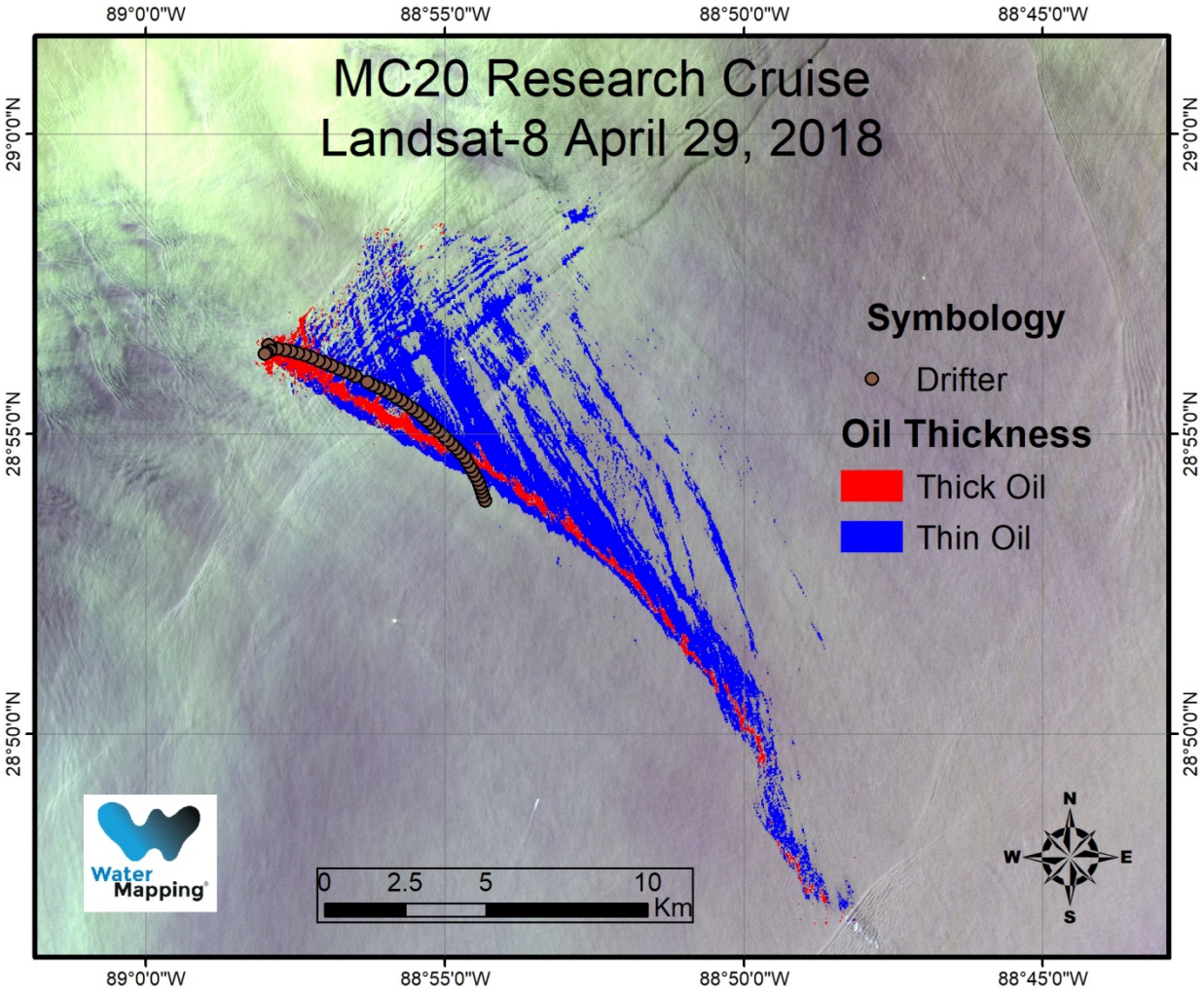


Figure 40. Case 5 of drifter deployments with oil thickness classification.

A high-resolution image collected by Sentinel-2A is shown on Figure  below. This image shows the location of the drifter in reference to the thick oil, shown as a bright feature within the darker slick.

Figure 42 - Subset from Sentinel-2A that shows the position of the drifter after 3:20 hrs from its deployment at the source.

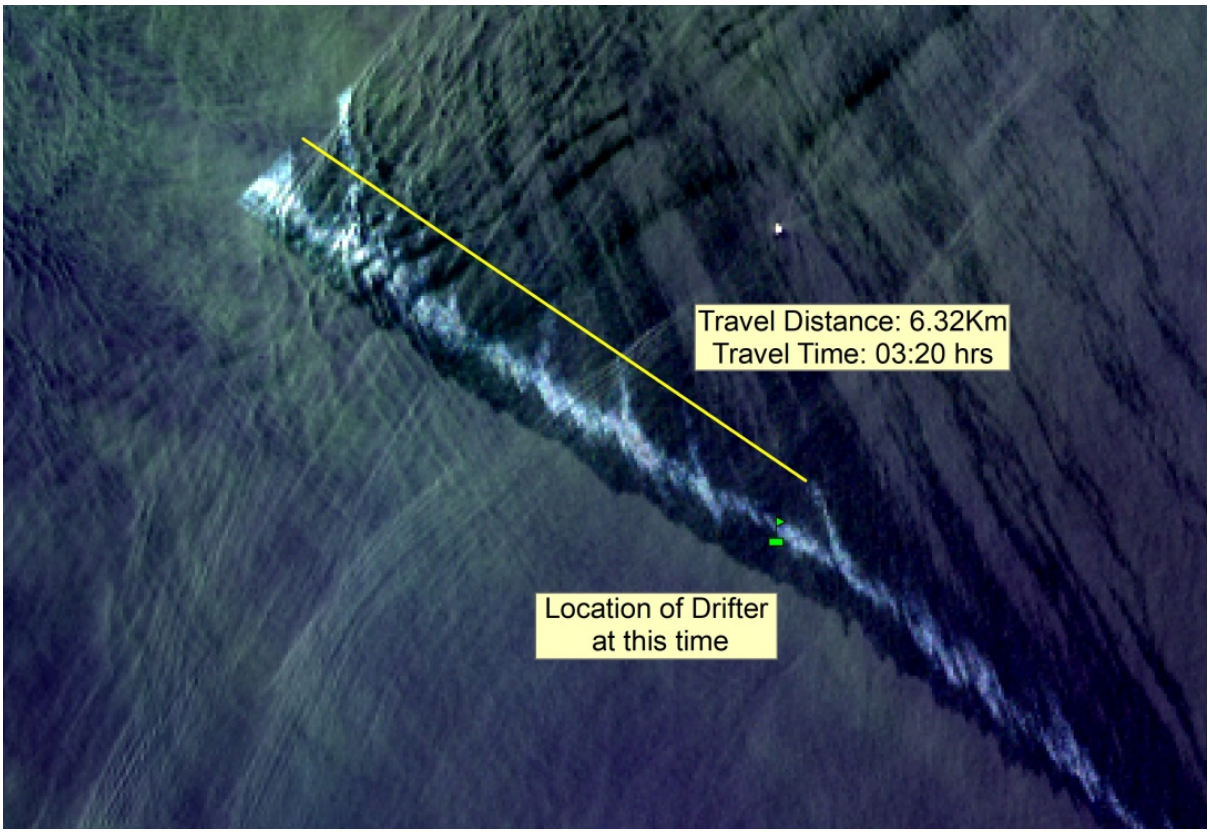


The total length of the slick for this case was 17km and the time that took the drifter to travel that distance was 15 hours. The average wind speed during that time was 3 m/s.

**Case 6. August 18, 2018.**

On our last deployment I was assisted by my colleagues from NOAA and the USCG on board of the USCG Brant. We arrived at the source of the slick and deployed an un-drogued drifter at 08:11 hrs (Figure 43). This drifter was constantly monitored by the UAS and we conducted multiple observations along its path for about 9 hours.

Figure 43. The USCG Brant monitoring around the oil source at MC20 guided by the UAS real time video system. A smaller zodiac boat was deployed with personnel from NOAA who collected additional net samples for chemical analysis.

Figure 44 below shows the USCG Brent drifting along the GPS drifter. We perform this monitoring operation for 9 hours. During this time we experienced thunderstorms and wind shear of 360 degrees. Outstandingly, on top of the rain, thunderstorms, and wind change in direction, the oil prevailed on the surface and the drifter stayed on the oil at all times, a fact we could confirm directly with the UAS.

By tracking its position, we retrieved the drifter on the next morning, and using the UAS we could confirm that oil was not present in the area anymore as it was fully evaporated and dissipated as expected (Figure 45).


Figure 45. Retrieval of the GPS drifter.

Table 6 shows a summary of the 6 cases where CARTHE un-drogued drifters were deployed at the origin of the MC20 site and were I tracked its displacement as they were captured by satellite imagery. This study allowed me to measure the distance the oil traveled in reference to the time that took the drifter to transit the same time under the same oceanographic and meteorological conditions as it was imaged by different satellites.

Table 6. Summary of the drifter deployments.

| Case | Oil displacement (km) | Average Wind (m/s) | Drifter Time (hrs) | Drifter Type | | | |
|---|---|---|---|---|---|---|---|
| | | | | CARTHE Un-Drogued | CARTHE DROGUED | IESPHERE MetOcean | CODE MetOcean |
| 20-Apr-2017 | 24.5 | 6.23 | 10 | 1 | 1 | 1 | |
| 25-Apr-2017 | 13.6 | 9.12 | 8 | 1 | 1 | | |
| 26-Apr-2017 | 8.9 | 10.1 | 6 | 1 | 1 | 1 | 1 |
| 16-Aug-2017 | 54 | 3 | 17 | 1 | 1 | 1 | 2 |
| 20-Apr-2018 | 17 | 3 | 15 | 1 | | | |
| 18-Aug-2018 | 11 | 4 | 14 | 1 | | | |
| AVERAGE | 20.9 | 5.84 | 11.66 | | | | |

The average of the oil slick length was 20.9 miles, and in average, the time that took drifters to be displaced this distance was approximately 12 hours, under average wind conditions of 5.84m/s

These cases basically confirm that wind is the main driving factor on the displacement of the surface oil. Not only because wind will guide the direction and speed of transport, but, more importantly, because the strength of the wind will be directly correlated with the evaporation ratio. The "Calm Wind Case" (Figure 39) confirmed that oil could travel for much longer periods of time if the wind is calm enough to let the oil prevail on the surface for longer periods of time. These calm wind conditions in combination with a strong current observed by the Mississippi River plume displaced the oil a distance of 54km in only 17 hours. This confirms the fact that when calm wind conditions persist oil will last longer on the surface. In contrast, the 'Strong Wind Case' (Figure 38), helped to confirm that under conditions like this (wind speed above 10m/s) the evaporation ratio will increase drastically and the displacement of the oil will increase on its speed as well. In that case oil was displaced 8.9km in approximately 6 hours.

This study confirmed the results obtained by other methods including hindcast modeling (as published by *Daneshgar et al*, 2017 and *MacDonald*, 2018). The average resident time on both approaches (Drifters and Hindcast modeling) show similar results. MacDonald (2018) used the same hindcast modeling technique from Daneshgar (2017) over MC20 slicks and calculated the same resident time of 12 hours.

**3.9 FLUID VOLUMETRIC FLOW RATE.**

The Fluid Volumetric Flow Rate (FVFR) of a system is a measure of the volume of fluid passing through a cross-sectional area per unit time. Based on my volume results presented on Section 3.7 (Minimum Volume = 19.86$m^3$, and Maximum Volume = > 55.42 $m^3$), and considering an average resident time of 12 hours, equal to 2 periods per day (or every 24hrs), the FVFR can be calculated as:

Minimum FVFR = 19.86 x 2 = 39.71 $m^3$/day (equivalent to 249 Barrels or 10492 gallons)

Maximum FVFR = >55.42 x 2 = 110.83 $m^3$/day (equivalent to 697Barrels or 29280 gallons)

**3.10 COMPARISON WITH NATIONAL RESPONSE CENTER (NRC) REPORTS.**

Data from records set forth on the United States Coast Guard's National Response Center webpage (See www.nrc.uscg.mil/) show daily reports from overflights about estimates of the oil volume from the MC20 site. Based on my review of the NRC reports and pilot observation forms used by Taylor Energy, it seems they might be using formulas that are not correct and misrepresent the amount of floating oil that can be observed from the MC20 site.

I gathered records from the NRC reports and matched those times where I had a satellite image during the same day (over the last couple years). A summary of these records can be seen on Table 7.

Table 7. Summary of NRC reports and Satellite observations.

| | Satellite Images | | From NRC reports |
|---|---|---|---|
| Date | Area (km2) | Volume Gallons | Volume Gallons |
| 5/23/2016 | 2.856193953 | 1553.769511 | 17.37 |
| 5/26/2016 | 8.407069402 | 4573.445755 | 137.78 |
| 6/3/2016 | 120.617229 | 65615.7726 | 41.2 |
| 6/23/2016 | 32.57849214 | 17722.69972 | 41.2 |
| 7/2/2016 | 23.78808486 | 12940.71816 | 33.47 |
| 7/21/2016 | 22.03264401 | 11985.75834 | 69.74 |
| 8/22/2016 | 26.11011543 | 14203.90279 | 107.73 |
| 9/2/2016 | 2.82032 | 1534.25408 | 324.7 |
| 11/17/2016 | 36.41714536 | 19810.92708 | 232.17 |
| 4/4/2017 | 2.863005891 | 1557.475205 | 81.01 |
| 4/18/2017 | 10.2658992 | 5584.649162 | 39.75 |
| 4/25/2017 | 17.79824608 | 9682.245865 | 73.45 |
| 8/14/2017 | 69.212186 | 37651.42918 | 380.87 |
| 9/1/2017 | 7.747103 | 4214.424032 | 122.59 |
| 10/13/2018 | 28.139067 | 15307.65245 | 103 |
| 12/12/2017 | 2.609811 | 1419.737184 | 0.1 |
| 2/10/2018 | 22.867447 | 12439.89117 | 1.44 |
| 4/13/2018 | 2.187083 | 1189.773152 | 13.33 |
| 4/30/2018 | 1.618633 | 880.536352 | 7.3 |
| 5/29/2018 | 4.867421 | 2647.877024 | 22.06 |
| 6/8/2018 | 12.176604 | 6624.072576 | 57.57 |
| 6/22/2018 | 48.05483 | 26141.82752 | 30.1 |
| 6/28/2018 | 11.294825 | 6144.3848 | 104.55 |
| 7/20/2018 | 22.096771 | 12020.64342 | 119.3 |
| 7/26/2018 | 35.517146 | 19321.32742 | 2.14 |
| 8/3/2018 | 11.15504 | 6068.34176 | 12.33 |
| 8/20/2018 | 52.479862 | 28549.04493 | 50.94 |

By plotting the calculated volumes on those matching dates between NRC reports and satellite observations there is a clear disagreement between the two types of observations (Figure 46). The three yellow highlighted days (November 17, April 25 of 2017, and April 30 2018) I was presently at the MC20 site performing studies.

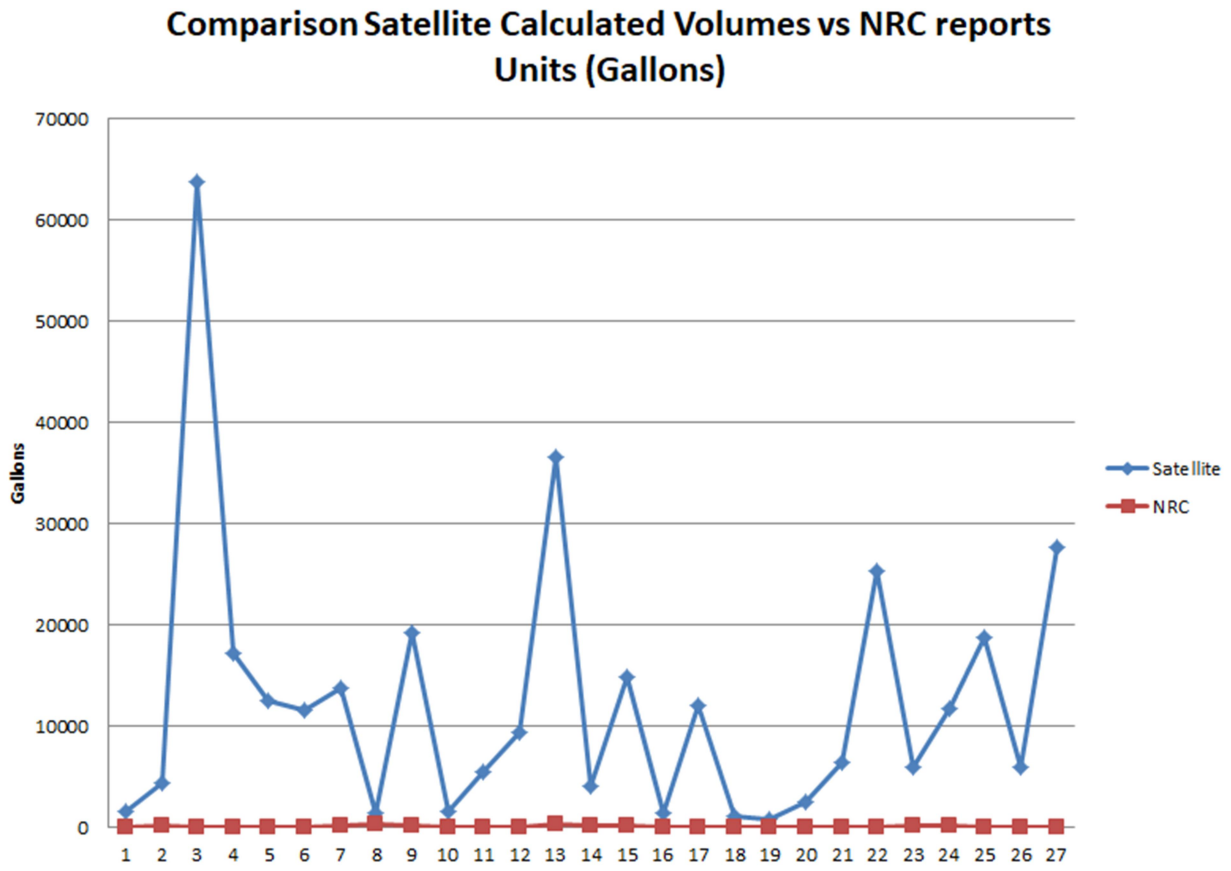


Figure 46. The difference between the estimated volumes from NRC and Satellite images is of several orders of magnitude.

For example, on November 17, 2017, I participated in an expedition where multiple entities (including NASA aircraft UAVSAR, NOAA, Ocean Imaging Inc., Fototerra, and Abt Associates) visited the site and utilized remote sensing technology to measure the presence of oil thicknesses and the extent of the slick originated by the MC20 site. Figure Figure 47 shows the extent of the slick measured by the NASA instrument UAVSAR.

Figure 47 - Image collected by NASA's instrument UAVSAR.

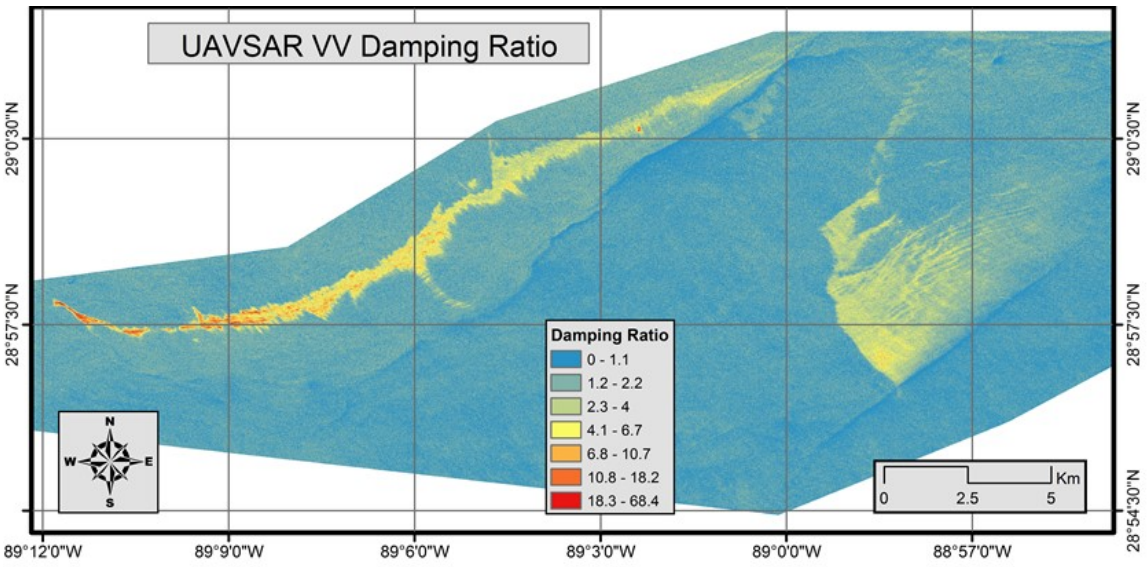


Figure 487 - Image collected by RADARSAT-2. At the same time as NASA instrument.

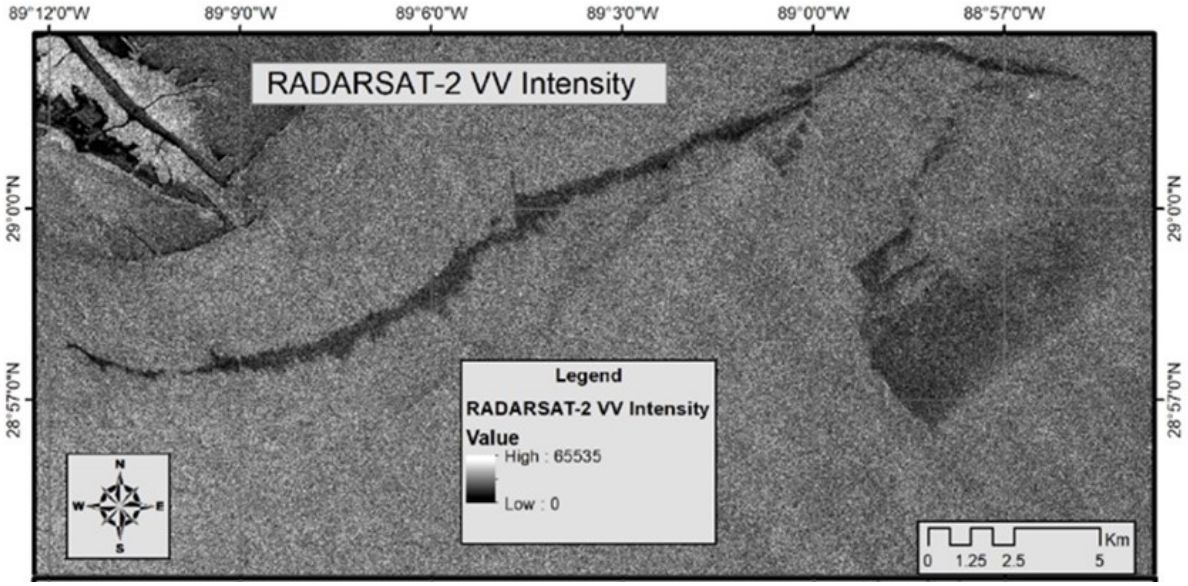


The flight of the UAVSAR was planned to acquire data at the same time that RADARSAT-2 collected a super high resolution image of the slick. These remote sensing technologies were used in coordination with me so that I could be on strategic locations of the slick at sea level to collect direct observations. I used an aviation radio to communicate directly with personnel onboard the NASA aircraft. Figure 48 shows the satellite image collected by RADARSAT-2.

These state of the art remote sensing technologies collected those datasets shown on the previous figures while I was collecting data with my UAS and thickness measurements with the WM-OST. This video link shows (see https://www.youtube.com/watch?v=Po01RZpB97g) the observations from the UAS collected in synchronization with the remote sensing data. Figure 49Figure 49  shows a sample of oil collected to retrieve the measurement of the oil slick thickness.

Figure 49 - Oil thickness sample for measuring the oil spill thickness.


A video that summarize the observations during this field campaign can be seen here https://www.youtube.com/watch?v=beMowmsNPCg

In summary, the use of sea level observations allowed me to apply measurements collected on the field into the satellite image collected by RADARSAT-2. The classification of the oil and its thickness is shown on Figure 50.

Figure 50 - After applying the algorithm known as Entropy from the Quadpol SAR data, the total volume calculated from the MC20 site captured by RADARSAT-2 was 72 m3 equivalent to over 19000 gallons floating on the ocean at the time of the satellite snapshot.

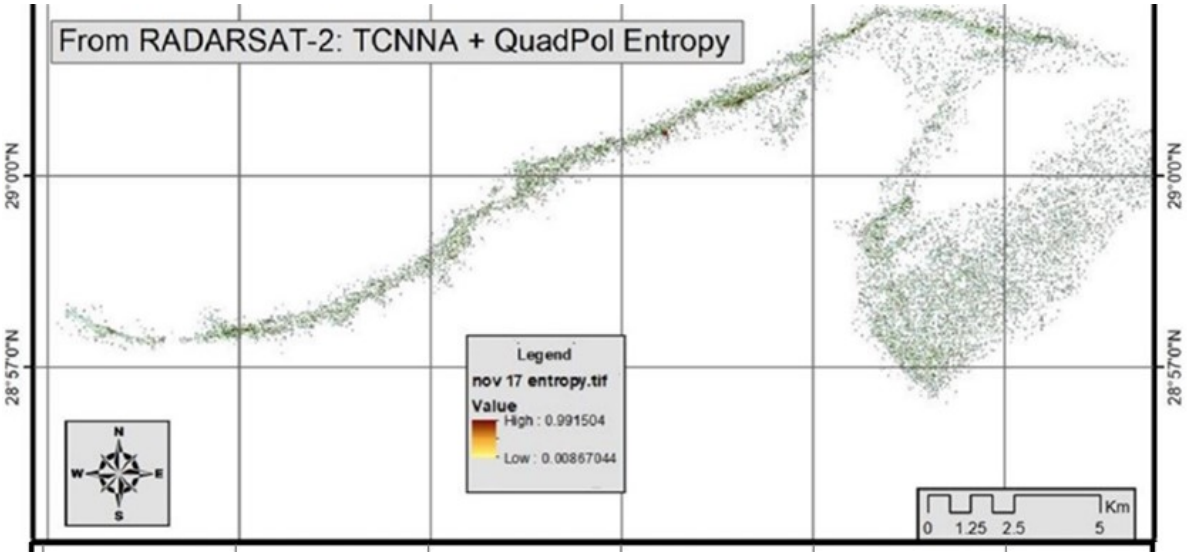


The NRC reported 232 gallons based on their areal observation. Based on the information presented here, my conclusion is that NRC reports are not reliable as there is a remarkable difference on the estimates (232 vs 19000 gallons). This discrepancy is persistent during other occasions where I was collecting data on the field and, it persists on all of the days where satellite images are available.

### 3.11 OIL FLUX OVER TIME

Analysis of the satellite imagery over time allows us to compare the area extents of the slicks (in average) year after year. Figure 51 shows that the area extent of the slicks have been within a range between 23 to 47 $km^2$. Over the last two years there has been a clear up trend in the size of the slicks on average.

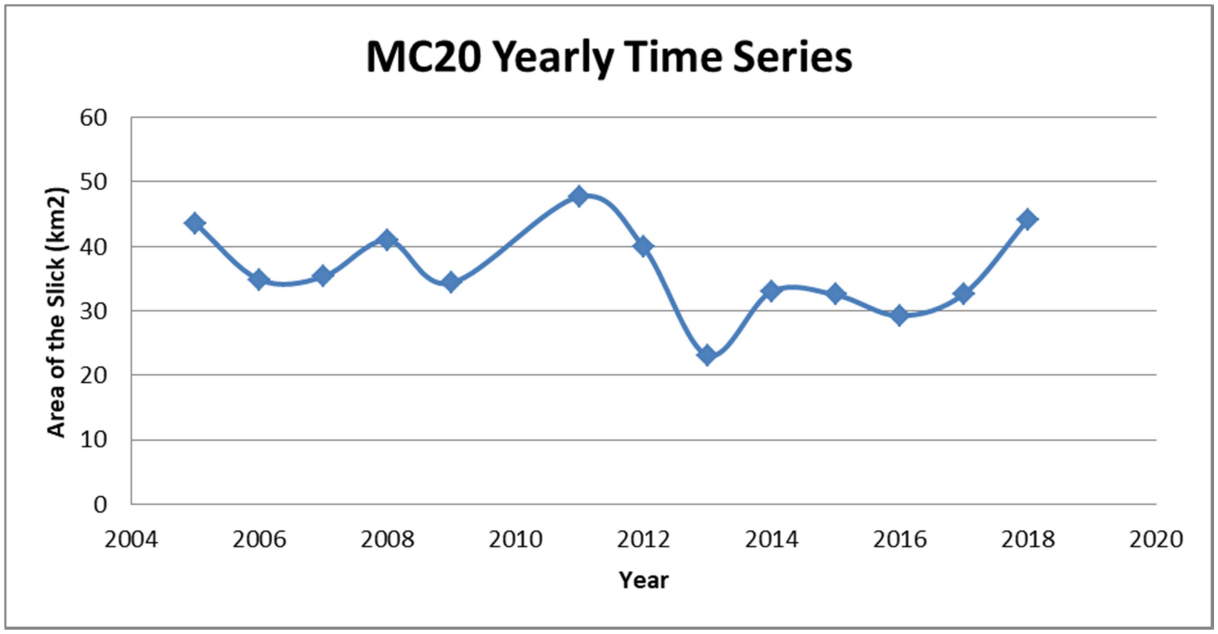


In order to resolve this variability more accurately, further investigation would be required to only consider images that fall within the range of wind conditions of the drifter observations (between 3-10 m/s), so, that we can monitor the volumes without being biased by images that are affected by storms or strong wind conditions.

**3.12 CONCLUSIONS**

It is my opinion that the amount of oil being discharged from Taylor MC20 site is at least between 249 and 697 barrels per day in average. The range in these numbers is based upon the application of minimum and maximum thicknesses of the oil as observed by satellites and using the Bonn Agreement Oil Appearance Code.

REFERENCES

Alpers, W., and H. Hühnerfuss (1988), Radar signatures of oil films floating on the sea surface and the Marangoni effect, *93*(C4), 3642-3648, doi:doi:10.1029/JC093iC04p03642.

Androulidakis, Y., Kourafalou, V., Özgökmen, T., Garcia-Pineda, O., Lund, B., Le Hénaff, M., Horstmann, J. (Accepted/In press). Influence of River-Induced Fronts on Hydrocarbon Transport: A Multiplatform Observational Study. *Journal of Geophysical Research: Oceans*. DOI: 10.1029/2017JC013514

Caruso, M. J., M. Migliaccio, J. T. Hargrove, O. Garcia-Pineda, and H. C. Graber (2013), Oil Spills and Slicks Imaged by Synthetic Aperture Radar, *Oceanography*, *26*(2), 112-123.

Daneshgar, S., D. Dukhovskoy, M. Bourassa, and I. Macdonald (2016), *Hindcast modeling of oil slick persistence from natural seeps*, doi:10.1016/j.rse.2016.11.003.

Gade, M., W. Alpers, H. Hühnerfuss, H. Masuko, and T. Kobayashi (1998), Imaging of biogenic and anthropogenic ocean surface films by the multifrequency/multipolarization SIR-C/X-SAR, *Journal of Geophysical Research: Oceans*, *103*(C9), 18851-18866, doi:10.1029/97JC01915.

Garcia-Pineda, I. R. MacDonald, X. Li, C. R. Jackson, and W. G. Pichel (2012), Oil Spill Mapping and Measurement in the Gulf of Mexico With Textural Classifier Neural Network Algorithm (TCNNA), *IEEE Journal of Selected Topics in Applied Earth Observations and Remote Sensing*, *6*(6), 2517-2525, doi:10.1109/JSTARS.2013.2244061.

Garcia-Pineda, O., J. Holmes, M. Rissing, R. Jones, C. Wobus, J. Svejkovsky, and M. Hess (2017), Detection of Oil near Shorelines during the Deepwater Horizon Oil Spill Using Synthetic Aperture Radar (SAR), *Remote Sensing*, *9*(6), doi:10.3390/rs9060567.

Garcia-Pineda, O., I. MacDonald, C. Hu, J. Svejkovsky, M. Hess, D. Dukhovskoy, and S. Moorey (2013), Detection of floating oil anomalies from the Deepwater Horizon oil spill with synthetic aperture radar., *Oceanography*, *26*(2), 124-137, doi:https://doi.org/10.5670/oceanog.2013.38.

Garcia-Pineda, O., B. Zimmer, M. Howard, W. Pichel, X. Li, and I. R. MacDonald (2009), Using SAR images to delineate ocean oil slicks with a texture-classifying neural network algorithm (TCNNA), *Canadian Journal of Remote Sensing*, *35*(5), 411-421, doi:10.5589/m09-035.

Hu, C., X. Li, W. G. Pichel, and F. E. Muller-Karger (2009), Detection of natural oil slicks in the NW Gulf of Mexico using MODIS imagery, *Geophysical Research Letters*, *36*(1), doi:10.1029/2008GL036119.

Igor, I., H. Lars, K. Lev, W. Cecillie, and R. Johannes (2012), Comparison of Operational Oil Spill Trajectory Forecasts with Surface Drifter Trajectories in the Barents Sea, *Journal of Geology & Geophysics*, *1*(105).

Leifer, I., et al. (2012), State of the art satellite and airborne marine oil spill remote sensing: Application to the BP Deepwater Horizon oil spill, *Remote Sensing of Environment*, *124*, 185-209, doi:10.1016/j.rse.2012.03.024.

Liu, Y. Y., R. H. R. H. Weisberg, C. C. Hu, C. C. Kovach, and R. R. RiethmüLler (2013), Evolution of the Loop Current System During the Deepwater Horizon Oil Spill Event as Observed With Drifters and Satellites, *Monitoring and Modeling the Deepwater Horizon Oil Spill: A Record-Breaking Enterprise*, doi:doi:10.1029/2011GM001127 10.1029/2011GM001127.

MacDonald, I. R., et al. (2015), Natural and unnatural oil slicks in the Gulf of Mexico, *Journal of Geophysical Research: Oceans*, *120*(12), 8364-8380, doi:10.1002/2015JC011062.

MacDonald, I.R., (2018) Remote Sensing of Persistent Oil Slicks in Mississippi Canyon 20. Gulf of Mexico Oil Spill Ecosystem Conference. 2018. New Orleans.

MDA (2015), Characterization and Trajectory Modelling of Oil Slicks to Increase the Efficiency and Effectiveness for Oil Spill Response*Rep.*, 687 pp.

Reed, M., A. Turner, and A. Odulo (1994), *The Role of Wind and Emulsification in Modeling Oil Spill and Surface Drifter Trajectories*, 143-157 pp., doi:10.1016/1353-2561(94)90022-1.

Schuler, D. L., J. Lee, and K. W. Hoppel (1993), Polarimetric SAR image signatures of the ocean and Gulf Stream features, *IEEE Transactions on Geoscience and Remote Sensing*, *31*(6), 1210-1221, doi:10.1109/36.317442.

Sun, S., and C. Hu (2015), Sun glint requirement for the remote detection of surface oil films, *Geophysical Research Letters*, *43*(1), 309-316, doi:10.1002/2015GL066884.

Sun, S., C. Hu, L. Feng, G. A. Swayze, J. Holmes, G. Graettinger, I. MacDonald, O. Garcia, and I. Leifer (2016), Oil slick morphology derived from AVIRIS measurements of the Deepwater Horizon oil spill: Implications for spatial resolution requirements of remote sensors, *Marine Pollution Bulletin*, *103*(1), 276-285, doi:https://doi.org/10.1016/j.marpolbul.2015.12.003.

Svejkovsky, J., M. Hess, J. Muskat, T. J. Nedwed, J. McCall, and O. Garcia (2016), Characterization of surface oil thickness distribution patterns observed during the Deepwater Horizon (MC-252) oil spill with aerial and satellite remote sensing, *Marine Pollution Bulletin*, *110*(1), 162-176, doi:https://doi.org/10.1016/j.marpolbul.2016.06.066.

Svejkovsky, J., W. J. Lehr, J. Muskat, G. Graettinger, and J. Mullin (2012), *Operational Utilization of Aerial Multispectral Remote Sensing during Oil Spill Response: Lessons Learned During the Deepwater Horizon (MC-252) Spill*, 1089-1102 pp., doi:10.14358/PERS.78.10.1089.

Valenzuela, R. G. (1978), Theories for the interaction of Electromagnetic and ocean waves-A review, *Boundary Layer Meteorology*, *13*, 61-85.

APPENDIX A – Curriculum Vitae

APPENDIX B - Standards

APPENDIX C – Overview Maps

APPENDIX D – Reference Videos

APPENDIX E – Article Drifters

APPENDIX F – NRC reports